The Development and Analysis of a Generic Talus Bone Prosthetic

by

Alexandra Trovato

A thesis submitted in partial fulfillment of the requirements for the degree of

Doctor of Philosophy

in

Structural Engineering

Department of Civil and Environmental Engineering
University of Alberta

Abstract

Talar collapse results in incongruity of the ankle joint, resulting in pain, stiffness, and disability. In the past, standard treatment has been surgical fusion or total ankle arthroplasty. These treatments can result in a loss of motion and function of the foot, as well as pseudarthrosis. A solution to the problems associated with these treatments is a talar body implant that replaces the avascular portion of the talus or the talus in its entirety. Presently, there are reports of custom talar implants surgically implanted in patients; however, custom implants increase time between injury and surgery which makes this procedure a less desirable option. This study explores the feasibility of developing a generic talus bone prosthetic for patients in need of talar replacements.

The first step in the study was to determine the geometric variation between the shapes of 91 individual tali. Comparisons between three-dimensional geometric talus models were conducted to determine if different tali could be considered the same shape. From these models, the best shape was determined for the female and male template and the two were compared to determine if a unisex implant was feasible. One shape was found for the talus and a unisex implant template in ten sizes was created and found sufficient. The geometric template for the talar implant in multiple sizes was validated by comparing the template to the models.

A finite element (FE) model of the ankle joint, calcaneus, and navicular was created and used to investigate the change in contact pressure and distribution on the cartilage surfaces surrounding the talus when a biological talus, a custom, and a generic talar implant were placed in the joint. The results showed that the contact patterns on the surrounding cartilage from the custom implant closely resembled that of the biological talar body patterns, but with smaller areas of higher contact pressures. Although the contact patterns from the generic implant were slightly

different than those caused by the biological talus, contact areas and pressures were closer to the biological talus in magnitude than the custom implant. The FE model created was validated by comparing its results to cadaveric results from previous studies. The FE results indicated that a well-designed and appropriately sized generic talus implant closely mimics the original biological talus in terms of contact pressure intensity and distribution.

Joint compatibility of the generic implants was verified in human cadaver and FE studies. The implants for the right ankle for ten cadaveric specimens were 3D printed. The cadaveric ankles were scanned with the biological talus in the joint and thereafter with the implant in place of the biological talus. The scans were 3D modelled and the location of the implant within the ankle joint was compared to the location of the biological talus. Seventy percent of the deviations on the talar dome between the biological talus and implant were within the acceptable range. The deviations correlated with the contact areas caused by a 2000N axial load (determined through the FE study). Results showed that there would not be excessive pressure caused by a generic implant.

A case study explored the possibility of surgically implanting a generic talus bone prosthetic in a patient with bilateral talar avascular necrosis and collapse of the talar domes. A custom implant was created using CT scans of the patient's talus, tibia and fibula. The custom and generic implants were compared with the intact portion of the biological talus to determine how the implants would articulate with the calcaneus and navicular. The talar domes of the custom and generic implants were compared to the collapsed domes to determine how the width and height of the dome differed from the collapsed (biological) talar dome. The extreme width of the biological talus and implants were found to determine if the implants would fit in the ankle mortise. Both the generic and custom implant were found to be in the acceptable range deviation

range of 1mm, and as such either implant would be acceptable for implantation in the patient to maintain geometric compatibility of the ankle joint.

This research demonstrated that a generic talar implant could be a viable option for those in need of a talar replacement.

Preface

This thesis is an original work by Alexandra Trovato. The research project, of which this thesis is a part, received research ethics approval from the University of Alberta Health Research Ethics Board - Health Panel, Project Name "Determination of talar dimensions", No. Pro00026057, October 26, 2015.

Chapter 3 of this thesis is under review with the Journal of Foot and Ankle Surgery as A. Trovato, M. El-Rich, S. Adeeb, S. Dhillon, and N. Jomha "Geometric Analysis of the Talus and Development of a Generic Talar Prosthetic", manuscript FAS-D-16-00068. A. Trovato, M. El-Rich, and S. Adeeb designed the methodology. S. Dhillon and N. Jomha obtained the CT scans and consulted on the reading of the scans. N. Jomha provided the problem and the background. A. Trovato carried out the methodology and analysis. A. Trovato, M. El-Rich, S. Adeeb and N. Jomha reviewed the results and developed the conclusions. A. Trovato and M. El-Rich prepared the manuscript with assistance from S. Adeeb and N. Jomha. A. Trovato, S. Adeeb and N. Jomha obtained funding.

Chapter 4 of this thesis has been submitted to the Journal of Biomechanics as A. Trovato, M. El-Rich, D. Widmer, S. Adeeb, and N. Jomha "Finite Element Analysis of a Generic and Custom Talar Prosthetic Compared to a Biological Talus". A. Trovato and M. El-Rich designed the methodology. N. Jomha obtained the CT scans and provided the problem and the background. A. Trovato carried out the methodology and analysis. A. Trovato, M. El-Rich, S. Adeeb and N. Jomha reviewed the results and developed the conclusions. A. Trovato, D. Widmer, and M. El-Rich prepared the manuscript with assistance from S. Adeeb and N. Jomha. A. Trovato, S. Adeeb and N. Jomha obtained funding.

Chapter 5 of this thesis will be submitted to the Journal of Clinical Biomechanics as A. Trovato, M. El-Rich, T.D. Bornes, S. Dhillon, S. Adeeb, and N. Jomha "Analysis of a Generic Talar Prosthetic with a Biological Talus: A Cadaver Study". A. Trovato, M. El-Rich, and S. Adeeb designed the methodology. A. Trovato, T.D. Bornes, and N. Jomha carried out the methodology. S. Dhillon and N. Jomha obtained the CT scans and consulted on the reading of the scans. N. Jomha provided the problem and the background. A. Trovato carried out the analysis of the data. A. Trovato, M. El-Rich, S. Adeeb and N. Jomha reviewed the results and developed the

conclusions. A. Trovato and M. El-Rich prepared the manuscript with assistance from S. Adeeb and N. Jomha, and T.D. Bornes. A. Trovato, S. Adeeb and N. Jomha obtained funding.

Chapter 6 of this thesis will be submitted to Annals of Biomedical Engineering as A. Trovato, M. El-Rich, A. Grosvenor, S. Adeeb, and N. Jomha "A Generic Talar Prosthesis for Bilateral Talar Collapse". A. Trovato and M. El-Rich designed the methodology. N. Jomha and A. Grosvenor obtained the CT scans and consulted on the reading of the scans. N. Jomha provided the problem and the background. A. Trovato carried out the methodology and analysis. A. Grosvenor developed the custom implant. A. Trovato, M. El-Rich, S. Adeeb, A. Grosvenor and N. Jomha reviewed the results and developed the conclusions. A. Trovato and M. El-Rich prepared the manuscript with assistance from A. Grosvenor, S. Adeeb and N. Jomha. A. Trovato, S. Adeeb and N. Jomha obtained funding.

This thesis is an original work by Alexandra Trovato. No part of this thesis has been previously published with the exception of the aforementioned.

Acknowledgements

I would like to thank my supervisory committee Dr. Marwan El-Rich, Dr. Samer Adeeb, and Dr. Nadr Jomha for sharing their knowledge with me and for providing support throughout my studies. I appreciate all of the time and effort you have invested in this research and in me. I would especially like to thank Dr. El-Rich for his invaluable help and patience during the computer simulation phase in the final stages of my program.

I would also like to thank my family and friends for their support during this journey. I would especially like to thank my husband (Steve), my parents (Nick and Chereda), my brothers (Cainan and Adam) and my in-laws (John and Gloria). Words cannot express how grateful I am to have had your love and encouragement throughout this time. I love you all so very much. Thank you for supporting me, listening to me complain, and pushing me when I needed it most. Most of all, thank you for putting up with me – this program was a challenge for me and I know that at times I wasn't easy on all of you. I promise that this is it – at least until the next challenge presents itself!

Table of Contents

List of Tables

List of Figures

Chapter 1 - Introduction

1.1 Problem Statement

Trauma to the talus bone can result in varying degrees of fractures, causing osteomyletis (infection and inflammation of the bone), malunion, and avascular necrosis (death of bone tissue due to a lack of blood supply.) It is therefore necessary to have a timely surgical treatment for this injury. Until recently, treatment of this injury has been limited to surgical fusion, which causes loss of motion and joint function (Barton, Lintz and Winson 2011) (Haddad, et al. 2007) (Hendrickx, et al. 2011). More recently, total ankle arthroplasties have been implemented with growing success. These arthroplasties, however, are not a conducive treatment for talar fractures that result in avascular necrosis. This is due to poor vascular status prior to operation and/or lack of bone stock required for the implant (Hintermann and Valderrabano 2003). As a result, the creation of a talar body implant is necessary to repair the joint and maintain joint function. In order to limit the time between injury and replacement of the talus (as prolonged time negatively affects the surrounding bone), and reduce costs associated with a custom-made talar implant, a generic prosthetic talus bone in different sizes would be preferable to a custom-made talus implant. As such, it is necessary to research if it is possible to create a generic prosthetic talus bone that can mimic the mechanical behaviour of the biological talus.

1.2 Objectives and Specific Aims

The overall objective of this study is to create a generic talar prosthesis in multiple sizes that can account for inter-individual ankle geometry variation, and maintain the function and geometric compatibility of that of a biological talus.

Objective 1: Determine the geometric variation between the shapes of individual tali. (Chapter 3)

Hypothesis: Tali can be divided into three groups: short and wide, long and narrow, and proportionate.

Specific Aim 1: Compare the shape of each male talus with other male tali and each female talus with other female tali.

Specific Aim 2: Classify the geometry of the talus into different shape groups.

(The results of Objective 1 indicated the failure of the hypothesis that different shape groups could be found among tali, so we proceeded with the following objectives:)

Objective 2: Develop a geometric template for the talar implant in multiple sizes. (Chapter 3)

Specific Aim 1: Identify the best shape for the talar implant for both the male and female talus.

Specific Aim 2: Determine the difference between the selected male and female implants.

Specific Aim 3: Determine the number of implant sizes.

Specific Aim 4: Validate the sizes by comparing the geometry of the individual tali with the implant in the correct size.

Objective 3: Develop a Finite Element (FE) model of the ankle joint to determine the contact pressures and areas on the articular cartilage surrounding the talus when a biological talus, custom implant, or generic implant is in the joint. (Chapter 4)

Specific Aim 1: Preparation of the model (which includes: boundary condition, material properties, loads) and validation study.

Specific Aim 2: Compare the contact pressures and areas caused by a generic implant, custom implant, or biological talus when the joint is under load.

Objective 4: Verify the joint compatibility of the talar implant using a cadaver study. (Chapter 5)

Specific Aim 1: Devise an experimental technique and a geometric model to compare the compatibility of the generic talar implant.

Specific Aim 2: Apply the geometric model to analyze the difference between the positions of the generic implant vs. the biological talus when in a cadaveric ankle joint.

Specific Aim 2: Determine if there are any correlations between contact areas (determined from FEA) and deviations between the biological talus and the generic implant.

Objective 5: Case study that explores the possibility of surgically implementing a generic talus bone prosthetic in a patient with bilateral talar avascular necrosis and collapse of the talar dome. (Chapter 6)

Specific Aim 1: Create a custom implant for the patient.

Specific Aim 2: Devise and implement an experimental technique and a geometric model to compare the geometric compatibility of the custom and generic talar implants.

1.3 Scope and Limitations

This research explored the possibility of creating a generic prosthetic talus bone to be used in talar replacement surgeries. The scope of the research included geometric analysis of human tali and the proposed generic prosthetic, as well as Finite Element Analysis (FEA) of the biological talus, custom implant, and generic implant. Limitations of this study include the following:

- The FE model studied the neutral position only.
- The cartilage on the bones was assumed to have a uniform thickness.
- The boundary conditions for the navicular bone and the calcaneus bone were fixed in place when in reality, there may be some relative movement allowed.

1.4 Research Contribution

This research will have major impact on the health of Canadians affected by talar fractures. Severe talar fractures typically occur in young, active individuals. Talar avascular necrosis with collapse results in significant disability. To enhance the patients' quality of life, the repair of such talar fractures is essential. As such, the development of a commercially viable generic prosthetic talus that is compatible with the population is important. The long-term objective of this research project is to create a new talar implant system based on rigorous computer analysis methods. The new technology will dramatically reduce the pre-operation preparation time. Additionally, it will reduce production cost of the implants as they will be able to be mass manufactured.

This research develops a generic implant based on scaling the cube root of the volume, and is the first of its kind that test the implant through geometric and cadaveric assessments, and FEA. Although there has been significant research focused on hips, knees and shoulders, there is considerably less information regarding the ankle joint. To our knowledge, this is the first study

to examine the effects on contact areas and pressures on the cartilage surrounding the talus when the talus is replaced with a titanium implant of the same geometry (a custom implant). Additionally, we are the first to examine the effect of introducing a generic implant in lieu of a custom implant.

Findings of this study were presented at the Congress of The European Society of Biomechanics and four manuscripts have been prepared and two have been submitted and are under review.

1.5 Outline of Thesis

This thesis includes 7 chapters.

Chapter 1

The problem statement, objectives, and specific aims of the current research are provided. The scope and limitations of the study are explained. The thesis chapters are presented with a brief explanation.

Chapter 2

A background on the anatomy of the talus bone and surrounding bones are described. Injury to the talus bone and its issues are discussed along with current surgical options available to those with talar injuries. Descriptions of previous studies conducted on the ankle are provided.

Chapter 3

The analysis is performed to determine if tali among humans can be considered the same shape, and as such, determines whether a generic implant can be created. This chapter also includes the analysis to determine if there are differences between the male and female talus and confirms that ten unisex implant sizes should be sufficient to maintain geometric compatibility of the ankle joint.

Chapter 4

FE models of the ankle joint with the calcaneus and navicular were created with three different tali – a custom implant, a generic implant, and the biological talus. The contact pressures and areas on the cartilage surrounding the talus in neutral position and under compressive load were

compared. A FE model of the talus bone and tibia was also created for validation purposes. Predictions of this model were validated against in-vitro data and compared to other FE results.

Chapter 5

A cadaveric assessment of the generic implant versus the biological talus is conducted using a geometric technique. Additionally, FEA is undertaken to determine if there is a correlation between FE results and how the generic implant sits in the cadaveric ankle joint relative to the biological talus. There is further discussion on whether a generic talar implant in ten unisex sizes will be feasible.

Chapter 6

A case study of a patient with bilateral talar collapse is presented. An analysis to determine if a generic implant will function geometrically the same as a custom implant is carried out.

Chapter 7

The findings of the thesis are summarized. Conclusions and recommendations for further research are provided.

References

Barton, T, F Lintz, and I Winson. "Biomechanical changes associated with the osteoarthritic, arthrodesed, and prosthetic ankle joint." Foot Ankle Surg 17, no. 2 (June 2011): 52-7.

Haddad, SL, JC Coetzee, R Estok, K Fahrbach, D Banel, and L Nalysnyk. "Intermediate and long-term outcomes of total ankle arthroplasty and ankle arthrodesis. A systematic review of the literature." J Bone Joint Surg Am 89, no. 9 (September 2007): 1899-905.

Hendrickx, RP, SA Stufkens, EE de Bruijn, IN Sierevelt, C van Dijk, and GM Kerkhoffs. "Medium- to long-term outcome of ankle arthrodesis." Foot Ankle Int 32, no. 10 (October 2011): 940-7.

Hintermann, Beat, MD, and Victor, MD Valderrabano. "Total Ankle Replacement." Foot Ankle Clin 8, no. 2 (June 2003): 375-405.

Chapter 2 - Background

2.1 Anatomy and Structure

2.1.1 Talus

The talus bone is a small, irregularly shaped bone. The talus is critical to the ankle joint because the unique shape controls the motion and interaction of the ankle and subtalar complex joints (Early 2008) (Kapandji 2011). It is also responsible for distributing the weight of the body over the entire foot (Chi and Schmitt 2005) (Mahato and Murthy 2012). Its surface area is approximately 70% covered with articular cartilage and has three articulating surfaces – the talar dome, subtalar area, and talar head which articulate with the tibia and fibula, calcaneus, and navicular respectively (Figure 2-1).

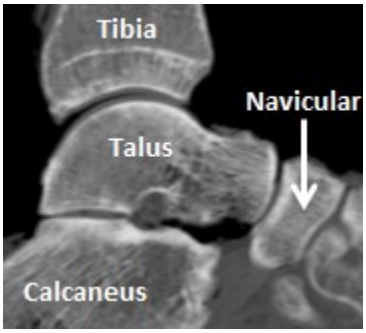

Figure 2-1: The talus and surrounding bones

The talus has no muscular attachment: it is sustained only by blood vessels coming in from ligament insertion sites (Figure 2-2) and a few direct blood vessels (Figure 2-3). This blood supply is just adequate under regular conditions. As a result, fractures of the talus can compromise the already delicate blood supply to the talus causing pseudarthrosis or avascular necrosis (AVN) (Kapandji 2011).

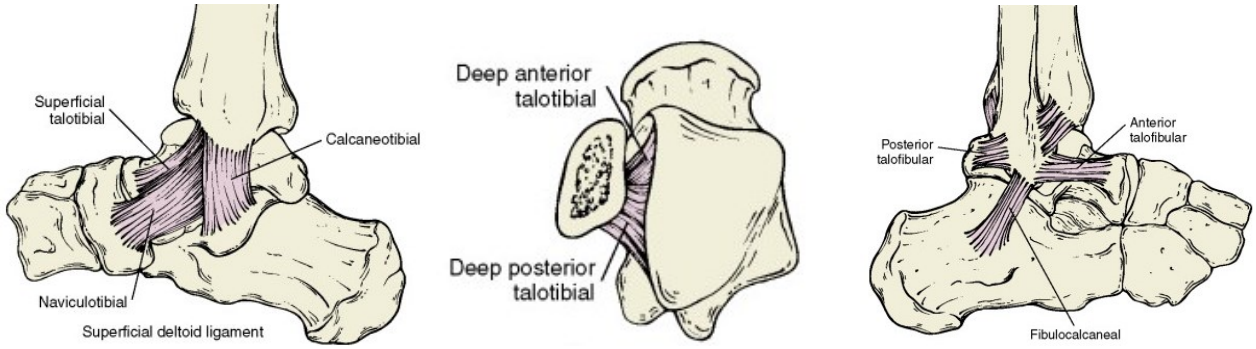

Figure 2-2: Superficial deltoid ligament, deep deltoid ligament and lateral collateral ligament (Carr 2009)

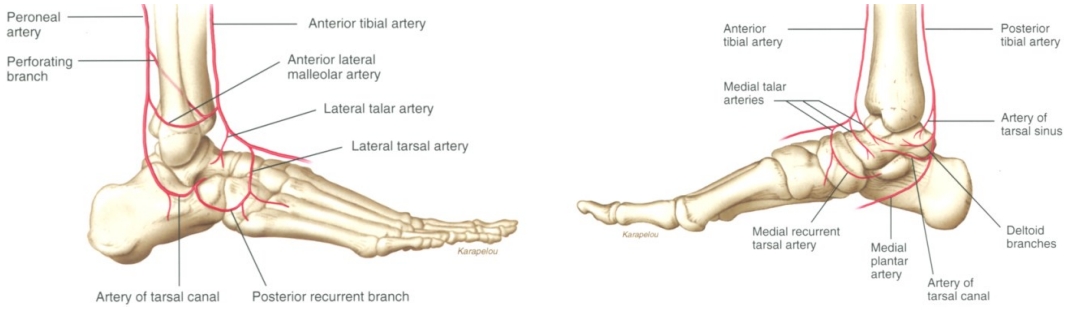

Figure 2-3: Blood supply to the talus – lateral and medial views (Smith and Ziran 1999)

2.1.2 Distal Tibia and Fibula

The tibia is the large medial bone of the leg and its inferior surface forms a hinge joint with the talus. The tibia passes the weight of the body across the talocrural joint (Martini, Timmons and Tallitsch 2006). The fibula parallels the lateral side of the tibia and the two are bound together by the crural interosseous membrane. The distal end of the tibia and fibula are also connected by the anterior and posterior tibiofibular ligaments. The medial malleolus of the tibia along with the lateral malleolus of the fibular process provide stability to the ankle joint, while the tibial plafond and the medial side of the lateral malleolus of the fibula are covered with cartilage (1.16±0.14mm and 0.85±0.13mm, respectively) and articulate with the talus (Martini, Timmons and Tallitsch 2006) (Millington, et al. 2007).

2.1.3 Calcaneus and Navicular

The calcaneus (heel bone) is the largest tarsal bone and the majority of one's weight is transferred from the talus to the calcaneus and then to the ground (Martini, Timmons and

Tallitsch 2006). The navicular bone articulates with the anterior surface of the talar head and is located on the medial side of the ankle; the distal surface of the navicular articulates with the three cuneiform bones that then articulate with the metatarsal bones of the foot (Martini, Timmons and Tallitsch 2006).

2.1.4 Cartilage

The talus, tibia, fibula, calcaneus, and navicular all have cartilage on their surfaces that articulate with other bones. Articular cartilage is the thin layer of fibrous connective tissue that transfers and distributes forces between articulating bones and joints, and allows relative movement between articular surfaces with minimal friction (Adeeb, et al. 2004) (Nigg and Herzog 1999). It is composed of cells (5%) and an intercellular matrix (95%) and is divided into four zones (the superficial zone, transitional zone, deep zone and calcified zone). When loaded, cartilage acts like a viscoelastic material; however, many researchers model cartilage as an equivalent linear elastic material (Adeeb, et al. 2004) (D. D. Anderson, J. K. Goldsworthy, et al. 2007) (Cheung, et al. 2005) (Ozkan, et al. 2013).

2.1.5 Male and Female Foot Bones

There are some indications in the literature that the foot bones may have slight differences between sexes that are not just due to size (Ferrari, et al. 2004). Ferrari et al analyzed angles and widths on the talus, the navicular, medial cuneiform, and the first metatarsal in the human foot to determine if there were differences between the male and female foot bones. Their main finding was that the majority of differences were principally due to size. Some angular measurments showed that there were some male-female differences specifically on the functional angles of the metatarsal head, medial cuniform, and talus indicating that the females may have slightly more movement in the joints.

2.2 Injury and Surgical Options

After calcaneus fractures, talus fractures are the most frequent of all tarsal bone fractures and account for 0.1-0.85% of all fractures (Bhandari and Adili 2011) (Huang and Cheng 2005) (Santavirta, et al. 1984). They are most common in a young, active patient population and are more likely to occur in men than women by a ratio of three to one (Bhandari and Adili 2011) (Thordarson 2007). Fractures of the talar neck, which account for approximately 50% of the

significant injuries to the talus (Thordarson 2007), can result in avascular necrosis in 20-100% of patients with displaced fractures. The avascular bone can be unsuitable to hold the required load and collapse can occur resulting pain, swelling, and restricted motion.

The most common surgical option in caring for this injury is ankle arthrodesis (fusion), wherein the talus is fused to the tibia or the tibia and calcaneus. Although arthrodesis often enables the patient to walk with decreased pain, the procedure results in loss of motion and function of the joint (Barton, Lintz and Winson 2011) (Haddad, et al. 2007).

Ankle arthroplasties have become a more desirable alternative to fusion as they have the potential to offer increased mobility of the ankle joint. Recently, they have been designed and implanted with increasing success (Kakkar and Siddique 2011). Ankle arthroplasties, however, are not suitable when the talar fracture results in AVN because the talus is often lacking the healthy bone stock that is required for talar fixation of the prosthesis.

An appropriate solution to the issues associated with arthrodesis and arthroplasties is a talar body implant that replaces the avascular portion of the talus, or the talus in its entirety, to maintain full ankle joint function. At this time, there have been some reports of talar body replacements. All implants have been custom made from various materials - stainless steel (Harnroongroj and Vanadurongwan 1997), alumina ceramic (Tanaka, et al. 2003) (Taniguchi, Takakura and Tanaka, et al. 2015), titanium alloy (Magnan, Facci and Bartolozzi 2004), and colbalt-chrome (B. W. Stevens, et al. 2007). The prostheses developed by Harnroongroj and Vanadurongwan (1997) were partial talar implants developed using custom measurements of volume and dimensions (including curvatures) of the contralateral talus; it was implanted in 16 patients. Tanaka et al (2003) developed prostheses similar to Harnroongroj and Vanadurongwan and implanted it in three patients (Figure 2-4). Both Magnan et al. and Stevens et al. replaced a talus utilizing CT scans to develop a prosthesis based on the real geometry of the bone. Taniguchi et al (2015) implanted 55 custom talus prostheses based on CT scans of the contralateral talus. All of these implants were custom-made and as such, involve increased time between injury and surgery, and are expensive.

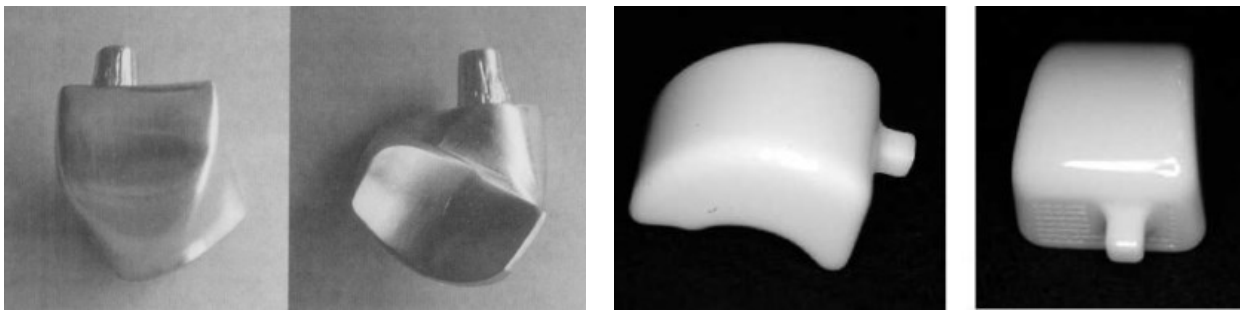

Figure 2-4: Harnroongroj and Vanadurongwan implant (left) and Tanaka et al. implant (right) (Harnroongroj and Vanadurongwan 1997) (Tanaka, et al. 2003)

The next step in the field of talus bone prosthetics would be the development of a generic talus bone prosthetic in different sizes to mitigate the costs and the extended time between onset of injury and surgery. This requires a generalization of the geometry of the talus.

2.3 Geometry and Generic Implants

The general shape of the talus has been defined in many anatomy and physiology texts. However, these texts offer general descriptions and illustrations of geometry with no specific ratios or dimensions (Kapandji 2011) (Martini, Timmons and Tallitsch 2006). Some researchers have attempted to describe the geometry of the talus and ankle joint but the majority of studies relied on two dimensional measurements and semi-automated measurements - tools that do not capture the complexity of the geometry of the talus bone (N. Mahato 2011) (Stagni, Leardini and Catani, et al. 2004) (Stagni, Leardini and Ensini, et al. 2005). Although a study has attempted to examine the 3D morphology of the ankle by determining anterior, middle, and posterior widths, as well as talar dome radii, it neglects to capture the full geometry of the talus and relies on anatomical landmarks (Hayes, Tochigi and Saltzman 2006). Statistical shape modelling has been widely used for interpreting and segmenting images, but is often reliant on using manually defined ‘landmarks’, which makes it prone to errors (Davis, et al. 2002) (Zhang, et al. 2012), and is difficult to do on a complex bone such as the talus. None of these previous studies have examined the shape of the talus when the tali are the same volume. Islam et al. first analyzed the geometry of the talus shape on 28 tali to determine if the shapes between tali were the same when scaled to the same volume and found that the shapes between tali were geometrically similar. This supports the development of a generic talar implant.

The creation of a generic talus bone implant in multiple sizes has been proposed in one previous study (K. Islam, et al. 2014). However, this study has limits, including the random selection of the implant shape, and an incremental jump in volume between sizes (which will be much more significant in the smaller sizes). Additionally, it lacks verification by a cadaveric study or computer modelling in relation to the surrounding bones and under loading.

2.4 Finite Element Simulations of the Foot

Most FEA of human joints have focused on the major articulation of the hips, knees and shoulders, with less information produced on the ankle joint (D. Anderson, et al. 2006). The literature has few FE studies that investigate ankle joint mechanics and most of these focus solely on the tibiotalar joint or on stress in the bones (D. D. Anderson, J. K. Goldsworthy, et al. 2007) (Cheung, et al. 2005) (Ozen, Sayman and Havitcioglu 2013) (Ozkan, et al. 2013) (Parr, et al. 2013).

Anderson et al (2007) completed a validation study for their FE model between the tibia and the talus using a Tekscan sensor under 600N of applied axial load on two cadaveric ankles. They focused their research on only the tibio-talar surface and found that they had good agreement between their FE-computed and experimentally measured mean (3.2% discrepancy for one ankle, 19.3% for the other) and maximum (1.5% and 6.2%) contact stress, and contact area (1.7% and 14.9%). Cheung et al (2005) created a robust FE model of the human ankle and complete foot with the distal tibia and fibula along with 26 foot bones and 72 major ligaments. They used their model to find interfacial pressures, von Mises stress in the bones and the strain of the plantar fascia. However, they did not measure the pressures on the cartilage in the talocrural, subtalar or talocalcaneonavicular joints. Ozkan et al (2013) created a complex FE model of the lower limb to calculate the differences in maximum equivalent stresses in the bones of the foot in patients with and without tibia vara (a growth disorder of the tibia). Although their model was complex, their measurements did not focus on pressures on cartilage, but stresses in the bones. Parr et al. (2013) conducted a FE study to research the importance of the trabecular geometry in FEA, with no focus or inclusion of on cartilage materials. Ozen et al. (2013) created a FE model of the human foot inclusive of soft tissue to determine the effects of a total ankle replacement on plantar pressure and von Mises stresses of the bones and prosthetic. To our knowledge, no other study has been conducted to determine the effects of the talus on the

surrounding cartilage surface. Furthermore, no one has investigated the effect on contact pressures and areas from using a whole talar implant, generic or custom.

References

Adeeb, Samer, Ezzeldin Y. Sayed Ahmed, John Matyas, David A. Hart, and Cyril B. Frank. "Congruency effects on load bearing in diarthrodial joints." Computer Methods in Biomechanics and Biomedical Engineering 7, no. 3 (2004): 147-157.

Anderson, Donald D., et al. "Intra-articular contact stress distributions at the ankle throughout stance phase--patient-specific finite element analysis as a metric of degeneration propensity." Biomech Model Mechanobiol. 5, no. 2-3 (2006): 82-89.

Anderson, Donald D., Jane K. Goldsworthy, Wendy Li, M. James Rudert, Yuki Tochigi, and Thomas D. Brown. "Physical validation of a patient-specific contact finite element model of the ankle." Journal of Biomechanics 40 (2007): 1662-9.

Barton, T, F Lintz, and I Winson. "Biomechanical changes associated with the osteoarthritic, arthrodesed, and prosthetic ankle joint." Foot Ankle Surg 17, no. 2 (June 2011): 52-7.

Bhandari, Mohit, and Anthony Adili. Evidence-based Orthopedics. Oxford: John Wiley & Sons, 2011.

Carr, James B. "Malleolar Fractures and Soft Tissue Injuries of the Ankle." In Skeletal Trauma, Fourth Edition, by Bruce D. Browner, Jesse B. Jupiter, Alan M. Levine, Peter G. Trafton and Christian Krettek, 2515-2584. Philadelphia, PA: SAUNDERS ELSEVIER, 2009.

Cheung, Jason Tak Man, Ming Zhang, Aaron Kam-Lun Leung, and Yu-Bo Fan. "Three-dimensional finite element analysis of the foot during standing--a material sensitivity study." Journal of Biomechanics 38 (2005): 1045-1054.

Chi, Kai Jung, and Daniel Schmitt. "Mechanical energy and effective foot mass during impact loading of walking and running." Journal of Biomechanics 38 (2005): 1387-1395.

Davis, R.H., C.J. Twining, T.F. Cootes, J.C. Waterton, and C.J. Taylor. "3D Statistical Shape Models Using Direct Length." Computer Vision — ECCV, April 29, 2002: 3-20.

Early, John S. "Talus Fracture Management." Foot Ankle Clin N Am 13 (2008): 635-657.

Ferrari, J, DA Hopkinson, and AD Linney. "Size and shape differences between male and female foot bones: is the female foot predisposed to hallux abducto valgus deformity." Journal of the American Podiatric Medical Association 94, no. 5 (2004): 434-52.

Haddad, SL, JC Coetzee, R Estok, K Fahrbach, D Banel, and L Nalysnyk. "Intermediate and long-term outcomes of total ankle arthroplasty and ankle arthrodesis. A systematic review of the literature." J Bone Joint Surg Am 89, no. 9 (September 2007): 1899-905.

Harnroongroj, T, and V Vanadurongwan. "The talar body prosthesis." J Bone Joint Surg Am. 79, no. 9 (Sep 1997): 1313-22.

Hayes, A, Y Tochigi, and CL Saltzman. "Ankle morphometry on 3D-CT images." The Iowa orthopaedic journal 26 (2006): 1-4.

Huang, PJ, and YM Cheng. "Delayed surgical treatment for neglected or mal-reduced talar fractures." Internal orthopaedics 29, no. 5 (Oct 2005): 326-9.

Islam, K, et al. "Three-dimensional geometric analysis of the talus for designing talar prosthetics." Proceedings of the 2014 combined Canadian Orthopaedic Association/American Orthopaedic Association (COA/AOA) and the Canadian Orthopaedic Research Society (CORS) Annual Meeting. Montreal: The Canadian Orthopaedic Association, 2014. 371-8.

Kakkar, Rahul, and MS Siddique. "Stresses in the ankle joint and total ankle replacement design." Foot and Ankle Surgery 17 (2011): 58-63.

Kapandji, AI. The Physiology of the Joints Volume Two The Lower Limb. Toronto: Elsevier, 2011.

Magnan, Bruno, Elisa Facci, and Pietro Bartolozzi. "Traumatic Loss of the Talus Treated with a Talar Body Prosthesis and Total Ankle Arthroplasty." The Journal of Bone and Joint Surgery, Incorporated 86-A, no. 8 (August 2004): 1778-82.

Mahato, N. "Morphology of sustentaculum tali: Biomechanical importance and correlation with angluar dimensions of the talus." The Foot 21 (2011): 179-83.

Mahato, Niladri Kumar, and Sathiya Narayana Murthy. "Articular and angular dimensions of the talus: inter-relationship and biomechanical significance." The Foot 22 (2012): 85-89.

Martini, Frederic H., Michael J. Timmons, and Robert B. Tallitsch. Human Anatomy. Fifth. San Francisco: Pearson Education Inc., 2006.

Millington, S.A., M. Grabner, R. Wozelka, D.D. Anderson, S.R. Hurwitz, and J.R. Crandall. "Quantification of ankle articular cartilage topography and thickness using a high resolution stereophotography system." OsteoArthritis and Cartilage, 2007: 205-211.

Nigg, Benno, and Walter Herzog. Biomechanics of the Musculo-skeletal System. Baffins Lane, Chichester: John Wile & Sons Ltd, 1999.

Ozen, Mustafa, Onur Sayman, and Hasan Havitcioglu. "Modeling and stress analyses of a normal foot-ankle and a prosthetic foot-ankle complex." ACTA of Bioengineering and Biomechanics 15, no. 3 (2013): 19-27.

Ozkan, Arif, Halil Atmaca, Ibrahim Mutlu, Talip Celik, Levent Ugur, and Yasin Kisioglu. "Stress distribution comparisons of foot bones in patient with tibia vara: a finite element study." Acta of Bioengineering and Biomechanics 15, no. 4 (2013): 67-72.

Parr, W. C. H, U. Chamoli, A. Jones, W. R. Walsh, and S. Wroe. "Finite element micro-modelling of a human ankle bone reveals the importance of the trabecular network to mechanical performance: new methods for the generation and comparison of 3D models." Journal of Biomechanics 46 (2013): 200-205.

Santavirta, S, S Seitsalo, O Kiviluoto, and P Myllynen. "Fractures of the talus." J Trauma 24, no. 11 (Nov 1984): 986-9.

Smith, Patrick N., and Bruce H. Ziran. "Fractures of the Talus." Operative Techniques in Orthopaedics 9, no. 3 (July 1999): 229-38.

Stagni, R, A Leardini, A Ensini, and A Cappello. "Ankle morphometry evaluated using a new semi automated technique based on X-ray pictures." Clinical biomechanics 20, no. 3 (Mar 2005): 307-11.

Stagni, R, A Leardini, F Catani, and A Cappello. "A new semi-automated measurement technique based on X-ray pictures for ankle morphometry." J Biomech 37, no. 7 (Jul 2004): 1113-8.

Stevens, Benjamin W., Christopher M. Dolan, John G. Anderson, and Charles D. Bukrey. "Custom Talar Prosthesis After Open Talar Extrusion in a Pediatric Patient." Foot & Ankle International, 2007: 933-8.

Tanaka, Y, et al. " Alumina ceramic talar body prosthesis for idiopathic aseptic necrosis of the talus." Key Engineering Materials, 2003: 805-8.

Taniguchi, A., et al. "An Alumina Ceramic Total Talar Prosthesis for Osteonecrosis of the Talus." J Bone Joint Surg Am, no. 97 (2015): 1348-53.

Thordarson, DB. "Talus fractures." FussSprungg 5 (2007): 104-13.

Zhang, K.Y., et al. "3D Morphometric and Posture Study of Felid Scapulae Using Statistical Shape ModellingX." PLoS One 7, no. 4 (2012).

Chapter 3 - Geometric Analysis of the Talus and Development of a Generic Talar Prosthetic

Abstract

Trauma to the talus can result in fracture, avascular necrosis and structural collapse. Treatment has been limited to surgical fusion and total ankle arthroplasty. Total ankle arthroplasty may not be an appropriate treatment for avascular necrosis while surgical fusion of the joint limits mobility. Custom-made implants have recently been used to address these limitations but have lengthy delays between injury and surgery and higher associated costs. A generic talar prosthesis available in various sizes may serve as a suitable alternative. The geometric variation between shapes of individual tali was determined using 3D geometric models of 91 tali created from CT-scan data. Comparisons were done to determine if tali are one shape. The best shape was determined for each sex, and was compared to determine if a unisex implant would be possible. A geometric template for the implant in multiple sizes was created and compared to the models. The average of the average deviation between tali after volume scaling was found to be less than 1mm on the articulating surfaces. One shape group was found for the talus. The female and male were found as the same and a unisex implant template was created. Ten implant sizes were found sufficient.

Keywords

Talus; generic prosthesis; deviation; geometric analysis

3.1 Introduction

Trauma to the talus bone can result in varying degrees of fractures. Due to the unusual vascular supply to this bone and its complex shape, healing problems such as malunion, and avascular necrosis (death of bone tissue due to a lack of blood supply) can occur. When significant avascular necrosis with collapse occurs, it results in severe incongruity of the joint resulting in pain, stiffness and disability. Standard treatment for this problem is surgical fusion of the tibia to the talus and the talus to the calcaneus (tibio-talo-calcaneal fusion). This type of surgical fusion results in severe loss of motion and function (Barton, Lintz and Winson 2011) (Haddad, et al. 2007) (Hendrickx, et al. 2011). More recently, total ankle arthroplasties have been implemented with growing success; however, these arthroplasties are not an appropriate treatment for talar fractures that result in avascular necrosis with collapse because the required bone stock required for embedding the implant is not available (Hintermann and Valderrabano 2003). Therefore, the creation of a talar body implant is an option to repair the joint and maintain proper joint function. In order to limit the time between diagnosis of talar body collapse and replacement of the talus (a delay which will make surgical reconstruction of the joint technically more difficult) and reduce costs associated with a custom-made talar implant, a generic talus bone prosthetic in different sizes would be superior to a custom made talus implant.

To create a generic talus prosthetic, detailed analysis of the talus geometry is required. The general shape of the talus has been defined in many anatomy and physiology texts; however, these texts offer general descriptions and illustrations of geometry with no specific ratios or dimensions (Kapandji 2011) (Martini, Timmons and Tallitsch 2006). Some researchers have attempted to describe the geometry of the talus and ankle joint but the majority of studies relied on two dimensional measurements and semi-automated measurements tools that do not capture the complexity of the geometry of the talus bone (N. Mahato 2011) (Stagni, Leardini and Catani, et al. 2004) (Stagni, Leardini and Ensini, et al. 2005). Although one study has attempted to examine the 3D morphology of the ankle by determining anterior, middle and posterior widths, as well as talar dome radii, it neglected to capture the full geometry of the talus and relied on anatomical landmarks (Hayes, Tochigi and Saltzman 2006). Additionally, none of these previous studies have examined the variation in shape of several tali when they are scaled to the same volume (size).

Islam et al. (2014) first analyzed the 3D geometry of 28 tali to determine if the shapes between tali were the same when scaled to the same volume and found that the shapes between tali can be considered geometrically similar. This supports the development of a generic talar implant. In this same study, Islam et. al (2014) proposed the creation of a generic talus bone implant in multiple sizes; however, this study had some limitations including the random selection of the implant shape, the incremental jump in volume between sizes (which will be much more significant in the smaller sizes), and a sample population that does not adequately represent that true population. In this paper we present a generic template for the talar implant in multiple sizes that can maintain the geometric compatibility of a biological talus.

3.2 Methods

3.2.1 Geometric Variation between the Shapes of Individual Tali

CT scans of intact, unfractured tali of 50 male tali (age 32.1±15.4 years) and 41 female tali (age 43.5±14.7 years) were obtained from the University of Alberta Hospital after ethical approval was obtained from the University of Alberta ethical review board. Each DICOM CT scan was imported into MIMICS (Materialize NV, Belgium), a medical image processing software. In MIMICS, a mask was created to cover the talus bone and from this mask, a 3D model was generated and imported into Geomagic Studio 2013 (Geomagic®, Morrisville, North Carolina; USA) for geometry cleaning and smoothing, and analysis.

To ensure that any deviations between tali were purely from shape and did not account for difference in size, each male and female talus was scaled to the same volume, using the scale factor below:

$$SF = \left(\frac{V_{av}}{V_x}\right)^{1/3}$$

$$where:$$

$$SF = scale\ factor\ for\ an\ individual\ talus$$

$$V_{av} = the\ average\ talus\ volume\ (male\ or\ female)$$

$$= \frac{\sum_{i=1}^{n} V_i}{n}$$

$$n = number\ of\ tali\ used\ in\ study$$

$$V_i = the\ volume\ of\ talus\ i$$

$$V_x = the\ volume\ of\ the\ original\ talus\ before\ scaling$$

After the scans were processed, modelled and scaled, each talus bone was compared with the remaining tali of the same sex. The tali were automatically aligned using the best fit approach built into Geomagic. The tali were then compared using the using the Geomagic 3D Compare Analysis and a deviation contour map was created. This process comparing one talus to another is illustrated in Figure 3-1. This process was repeated to create deviation maps between the 50 male and 41 female tali.

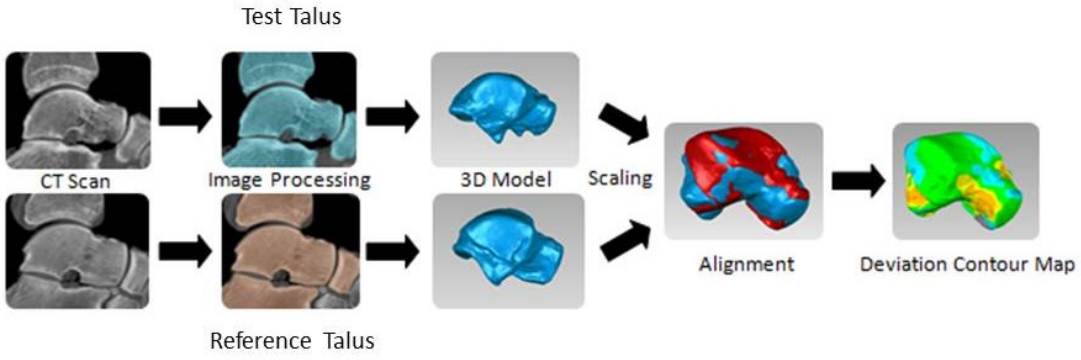

Figure 3-1: Flow diagram of modelling procedure (adapted from Islam, et al., 2014)

The results of this deviation analysis were summarized using 50 by 50 comparison matrices for the males and 41 by 41 comparison matrices for the females. The matrices illustrate the average deviations (d_{av}), maximum deviations (d_{max}), and standard deviation of the deviations, of each subject's talus compared with the other tali. The average of the average deviations (D_{av}) of each

talus as compared with the remaining tali of the same sex were calculated to determine if each talus is the same shape as the other tali. Tali were considered to be the same shape if the deviations on the articular surfaces are less than 1mm as a 1mm shift was recognized as the determining criterion for relocation of the talus after injury (Lloyd, et al. 2006). To determine if the tali were the same shape, the articular surfaces of the deviation contour maps (DCMs) were assessed.

To determine if multiple shape groups existed within our sample (or if there was just one shape group), an algorithm was implemented to group the tali into different shape groups. This algorithm split the male subjects into three equal groups that best matched each other (with lowest deviation). Originally, the first group was to be identified by dividing the number of subjects into 3 groups and finding the third of the subjects that best match each other; however, due to computing requirements, the sample size for the algorithm had to be reduced to 36 subjects. The sample size had to be reduced down from an initially proposed C_{16}^{50} to C_{12}^{36} due to the demands of performing 4.9236897e+12 operations. Looping through an array is an $O(n)$ operation which follows that the algorithm would evaluate to an $O(n^{16})$ time complexity. As such, it was necessary to reduce the initial sample size until a run time that completes within a reasonable human scale time period was achieved. The code was run such that the 12 subjects that best matched each other were selected to be representative of the first group (Group 1). These 12 subjects were then removed from the original 36 and the remaining 24 subjects were split in two equal groups that best matched each other forming Groups 2 and 3. The hypothesis was such that the most common, or average, shape would be selected in the first grouping (Group 1), while the remaining two-thirds of the subjects would then be a grouping of two extremes and thus, when selecting the best matches, the remaining tali would naturally be split into their respective extremes. The developed algorithm, illustrated below in Figure 3-2, took the random 36 by 36 matrix of the average deviations of the taluses and created all possible combinations of the 12 by 12 submatrices (C_{12}^{36}). The average deviation of each submatrix was calculated and the one with the lowest average deviation was selected. Consequently, the 12 subjects from this submatrix were selected as Group 1. This procedure was repeated with a 24 by 24 matrix (the 12 from Group 1 being removed) to split the remaining subjects into two groups. After the three groups were found, each talus was aligned in Geomagic to Subject 1 and a bounding box (a wire-framed box that indicates the maximum extents of an object) surrounding

the talus was measured to determine if the tali have been separated into different shapes. The dimensions from these bounding boxes were plotted against each other to determine if any trends exist.

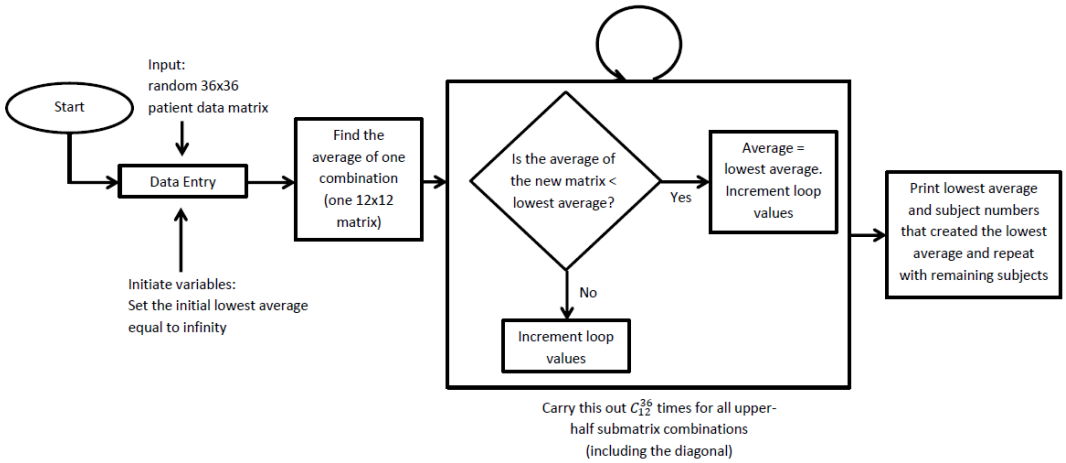

Figure 3-2: Talus grouping flow chart

3.2.2 Development of a Generic Talus Bone Implant

As will be shown in the results, no distinct groups were found for the tali shapes and thus an average shape for each sex was to be determined.

The best shape male and female talus was chosen by selecting the talus that has the lowest average deviation when compared to all of the tali of the corresponding sex. These best shapes were used for the implant templates. A comparison between the male and female implant templates, scaled to the same volume, was carried out as described earlier in the methodology. The purpose of the comparison was to investigate whether the variations between male and female implants warrant the creation of two different template shapes. As will be shown in the results, one unisex template was deemed appropriate for the implant shape.

The average volume (V_{avg}) of the 91 tali scanned was considered as the average volume of the population. An incremental jump in the cube root of the volume was applied to obtain the volume for each size as follows:

The cubic root of the mean volume ($\sqrt[3]{V_{avg}}$) was designated as the mean size. The standard deviation (σ) of the cubic roots of the volumes were calculated and used to obtain the different population sizes. The sizes were based on the addition and subtraction of standard deviations of the cubic roots of the volume to the cubic root of the mean volume.

Initially, six different sizes of the implant were created by scaling the volume of the implant shape. The range included $\sqrt[3]{V_{avg}} \pm 3\sigma$ in order to include the sizes found in over 99% of the population. However, a preliminary trial deviation comparison was performed and upon assessment of the deviation maps, it was evident that there were many locations on the talar dome that exceeded 1mm deviation. The talar dome is the main articulating surface in the ankle joint, and as such this part of the implant must have very low deviations when compared to the biological talus; the decision was made to increase the number of sizes to ten. The ten sizes and the distribution of sizes in our sample population are illustrated in (Table 3-1).

Table 3-1: Ten sizes for implants

Size	Number of subjects in size range	Range	Volume (mm^3)
1	1	$\sqrt[3]{V_{avg}} - 3\sigma < \sqrt[3]{V} \leq \sqrt[3]{V_{avg}} - 2.4\sigma$	20,246
2	1	$\sqrt[3]{V_{avg}} - 2.4\sigma < \sqrt[3]{V} \leq \sqrt[3]{V_{avg}} - 1.8\sigma$	23,463
3	8	$\sqrt[3]{V_{avg}} - 1.8\sigma < \sqrt[3]{V} \leq \sqrt[3]{V_{avg}} - 1.2\sigma$	27,005
4	18	$\sqrt[3]{V_{avg}} - 1.2\sigma < \sqrt[3]{V} \leq \sqrt[3]{V_{avg}} - 0.6\sigma$	30,886
5	22	$\sqrt[3]{V_{avg}} - 0.6\sigma < \sqrt[3]{V} \leq \sqrt[3]{V_{avg}}$	35,134
6	12	$\sqrt[3]{V_{avg}} < \sqrt[3]{V} \leq \sqrt[3]{V_{avg}} + 0.6\sigma$	39,742
7	17	$\sqrt[3]{V_{avg}} + 0.6\sigma < \sqrt[3]{V} \leq \sqrt[3]{V_{avg}} + 1.2\sigma$	44,736
8	10	$\sqrt[3]{V_{avg}} + 1.2\sigma < \sqrt[3]{V} \leq \sqrt[3]{V_{avg}} + 1.8\sigma$	50,132
9	2	$\sqrt[3]{V_{avg}} + 1.8\sigma < \sqrt[3]{V} \leq \sqrt[3]{V_{avg}} + 2.4\sigma$	55,946
10	0	$\sqrt[3]{V_{avg}} + 2.4\sigma < \sqrt[3]{V} \leq \sqrt[3]{V_{avg}} + 3\sigma$	62,192

3.3 Results

3.3.1 Geometric Variation between the Shapes of Individual Tali

The average volume of the male and female tali were 43,315mm^3 and 31,535mm^3, respectively. The average of the average deviation (D_{av}) between tali after volume scaling was 1.07mm between male tali and 0.87mm between female tali. The average deviations were found to be less than 1mm on the articulating surfaces of both sexes. A typical deviation map is shown in Figure 3-3.

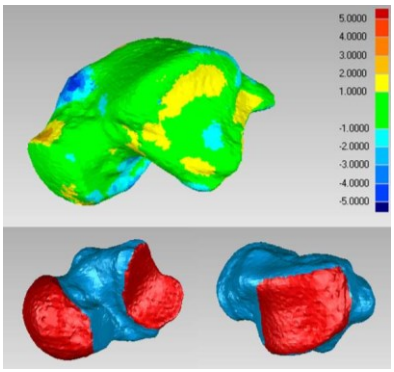

Figure 3-3: Deviation contour map between Subjects 1 and 72 when scaled to the same volume (articulating surfaces are shown in red in the bottom figure) (scale in mm)

The algorithm resulted in three shape groups. Groups 1, 2 and 3 had a D_{av} of 0.87mm, 1.00mm and 1.27mm among each group respectively. This indicated that the hypothesis of three different shape groups would fail as the D_{av} of each group became higher each time a group was removed. The sizes of the bounding boxes, illustrated in Figure 3-4, for each group are outlined in Table 3-2. The lengths, widths and heights of the bounding boxes were plotted to determine if there were any trends between groups and no trends were found (Figure 3-5, Figure 3-6, and Figure 3-7). Additionally, the lengths, widths, and heights of the bounding boxes are the same with less than a 4% difference between the averages and less than 1mm between the average dimensions of all groups (with the exception of the lengths between group 2 and group 3 which is 1.22mm). Therefore the conclusion was made that there are no distinctive shape groups within the talar geometry.

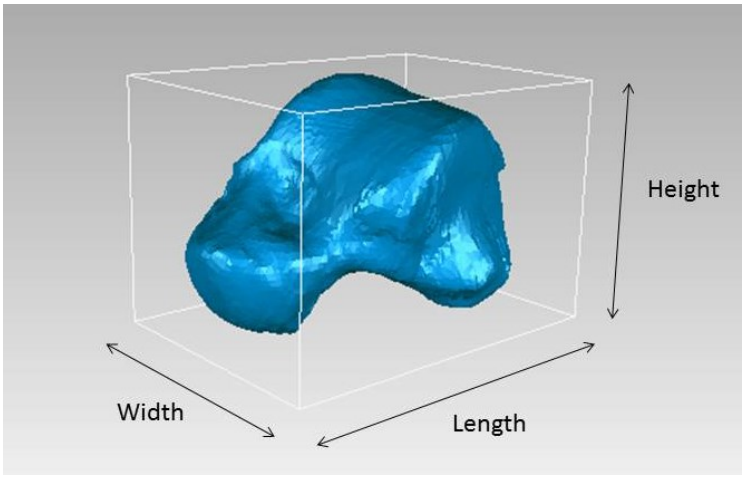

Figure 3-4: Illustration of the talar bounding box

Table 3-2: Bounding box sizes of the 3 groups (units in mm)

	Group 1			Group 2			Group 3		
	Width	Length	Height	Width	Length	Height	Width	Length	Height
Minimum	46.40	60.56	44.56	46.20	59.82	43.51	46.14	60.01	42.40
Maximum	48.98	66.71	46.37	49.50	66.07	46.72	49.56	67.38	47.47
Standard Deviation	0.78	1.98	0.63	0.98	1.83	0.88	1.11	2.15	1.35
Average	47.35	63.27	45.58	47.74	62.97	44.80	47.64	64.19	45.10

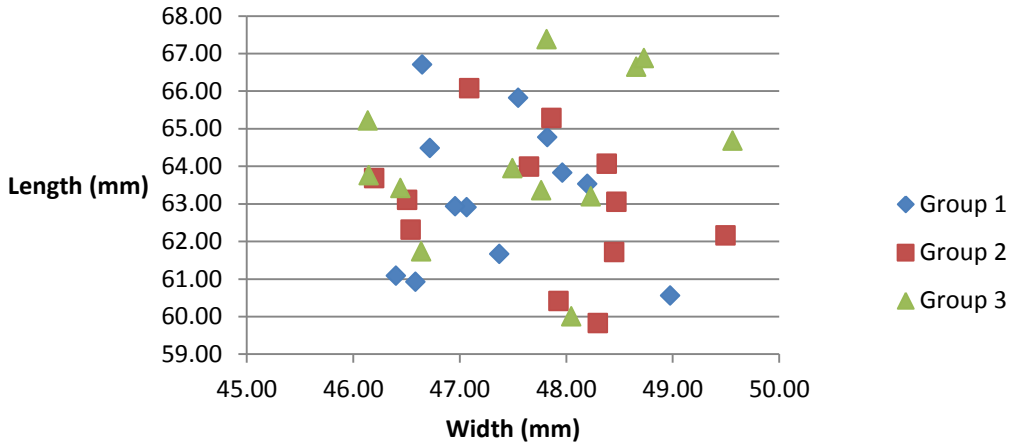

Figure 3-5: Bounding box width vs length

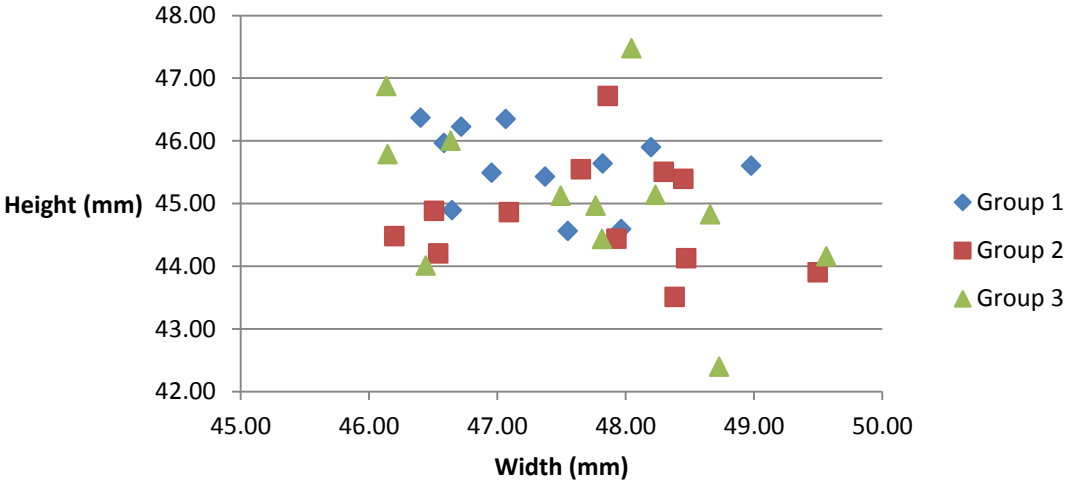

Figure 3-6: Bounding box width vs height

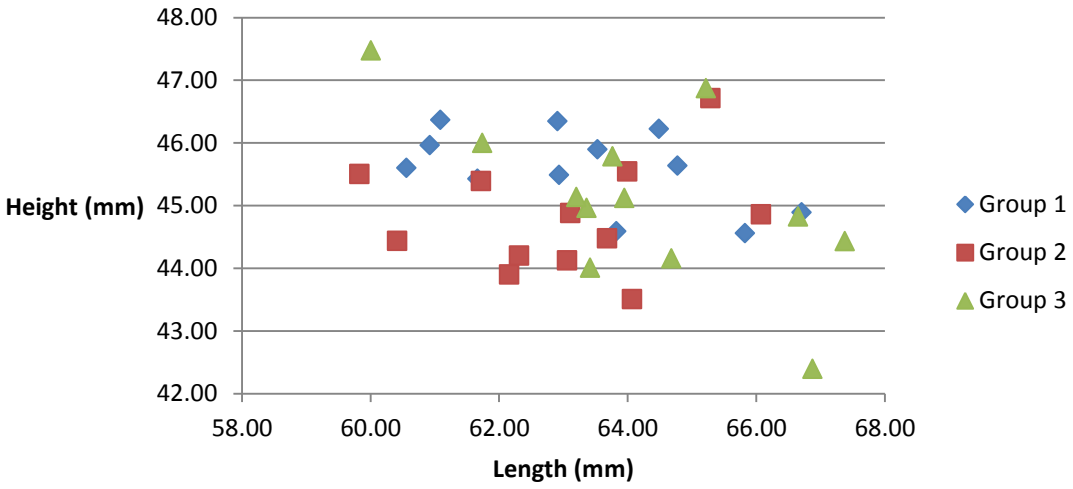

Figure 3-7: Bounding box length vs height

3.3.2 Development of a Generic Talus Bone Implant

The talus of subject 30 was chosen as the best male talus. This talus was one of the 12 selected in Group 1 which was hypothesized to be the most common, or average shape. It is also the talus that had the lowest D_{av} with the other subjects when all subjects are scaled to the same volume. This D_{av} between the chosen template and the remaining tali was 0.89±0.14mm. The talus of subject 15 was chosen as the best female talus. It is the female talus that had the lowest D_{av} with the other subjects when all subjects are scaled to the same volume. This D_{av} between the chosen template and the remaining tali was 0.75±0.11mm.

The best female talus volume was scaled to the same size as the best male talus. The average deviation between the two was 0.60mm, considerably less than the deviations seen between male vs male tali and female vs female tali. The DCM for the comparison between the male and female template is illustrated in Figure 3-8. Therefore, the female and male implants were considered to be the same and only one implant template will be used for both sexes – the male subject 30.

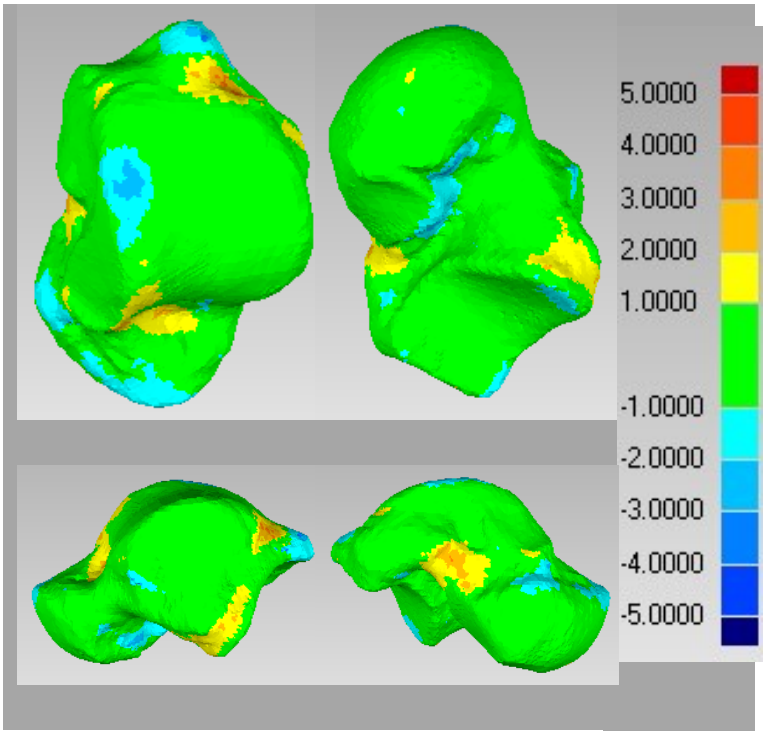

Figure 3-8: Male and female implant shape comparison (scale in mm)

The sizes were validated by comparing the talar dome of each of the 91 tali with the talar dome of the corresponding implant size. The average deviation between each talus and its respective size was found with an overall D_{av} of 0.88mm.

3.4 Discussion

The talus bone has a complex geometry and the ability to create a generic talus bone prosthetic requires a generalization of the talar geometry. Although some researchers have attempted to classify the geometry of the talus, the bulk of these studies relied on measurements tools that do not capture the talus bone's complex geometry and depend on anatomical landmarks that can be difficult to find consistently (N. Mahato 2011) (Stagni, Leardini and Catani, et al. 2004) (Stagni, Leardini and Ensini, et al. 2005) (Hayes, Tochigi and Saltzman 2006). One previous study analyzed the geometry of the talus shape and supported the development of a generic talar implant; however, the sample size in this previous study was small and did not adequately look at the female talus (K. Islam, et al. 2014). Additionally, this is the first study to investigate whether or not multiple shape groups for the talus may exist.

Statistical shape modelling has been widely used for interpreting and segmenting images; however, it is often reliant on using manually defined 'landmarks' which makes it prone to errors (Davis, et al. 2002) (Zhang, et al. 2012). This study proposes an alternative measure: to best-fit align the tali to the same talus and then implement a least-squares method for deviations which will result in accurate point to point differences along the entire dome without the use of landmarks that are prone to these errors. This method is also superior to looking at the curvature of the talar dome as the curvatures vary on different areas of the dome.

When the volumes of the tali were scaled to the same size i.e. volume (to ensure deviations due to size were ignored), the average deviations were found to be less than 1mm on the articulating surfaces of both sexes. Since a 1mm shift is recognized as the determining criterion for relocation of the talus after injury (Lloyd, et al. 2006), tali were considered to have the same shape if the deviations on the articular surfaces were less than this threshold. Results from this comparison were sufficient to preliminarily say that tali are the same shape among humans, which supports that the development of a generic talar implant would be possible. However, to ensure that the talus could not be classified further into more specific shapes, this study looked at whether or not shape groups existed within our sample by implementing an algorithm that split a sample population into three groups based on the tali that best match other tali in the group. Since there was found to be less than a 4% difference between the average dimensions of the bounding box for each shape group and less than 1mm between the average dimensions of all groups, it can be concluded that that there are no distinctive shape groups within the talar geometry.

The implants created for both the male and female tali were found by selecting the talus that had the lowest deviations compared to the other tali in each sex group. There are some indications in the literature that the foot bones may have slight differences between sexes that are not just due to size (Ferrari, et al. 2004). Ferrari indicated that there may be more movement in the female foot due to some slight differences in the angles of the foot bones (which would make females more predisposed to hallux abducto valgus formation). However, a comparison between the male and female implants, scaled to the same volume, showed that the deviations between the male and female implants were much smaller than within each sex indicating that for the purpose of this study, the female and male talus could be considered the same shape. Additionally, the

deviations between the female population (which were scaled to a smaller volume than the male population) were smaller than the deviations between the male population, which indicates that the deviations may be linked to the size that the talus is scaled to and not to the sex of the subject. However, the difference between male and female body weight effects on the mechanical response of the generic implant needs to be investigated.

The articulating surfaces on the talus are all important in considering a total talus bone replacement; however, the talar dome, which articulates with the tibia and fibula in the ankle joint, is of most importance because the ankle joint controls plantarflexion and dorsiflexion enabling walking. Therefore, the focus of implant testing was on comparing the talar dome of the 91 collected tali with the chosen average shape in the correct corresponding size. Based on the average deviations between the talar dome on the talus and the corresponding implant, it was determined through an iterative process (until the deviations were found to be acceptable) that the 10 sizes (that encompass over 99% of the sizes found in the population) were sufficient. Each talus from the study was compared with its corresponding implant size and from this analysis it was found that the an overall D_{av} between the tali and their corresponding size was 0.88mm (less than 1mm) indicating that this range of sizes would be feasible for geometric compatibility of the talus. However, it is important to note that a study conducted by Fregley et al. (2008) found that an accuracy of microns and milliradians is required to estimate contact forces, pressures, and areas directly (Fregly, et al. 2008); and as such, mechanical testing, modelling, or experimental analysis should be conducted to confirm this conclusion.

Islam et al. (2014) proposed an implant in multiple sizes; however, their study has limits that this paper addresses. The current study addresses these limits in three ways. Firstly, the female population is adequately represented with 45% of the subjects being female. Secondly, the current study carefully selected the implant shape by ensuring that the shape selected was the shape that most closely matched the other tali as opposed to selecting the template randomly. Finally, the current study used an incremental jump in cube root of the volume between sizes as opposed to an incremental jump in the volume. The limitation of using an incremental jump in the volume is that it will impart a significant effect on the smaller sizes. In other words, the smaller sized implants will have greater deviations between the implant and the original talus. However, similar deviations between the implant and the original talus across various sizes are

observed when the size changes are based on an incremental jump in the cube root of the volume.

Based on this research, we conclude that ten unisex implant sizes for the talus bone should be sufficient to maintain geometric compatibility of the ankle joint. These findings will be used in future studies to assess the feasibility of using this implant in a cadaver study, as well as using finite element analysis to investigate the redistribution of the contact pressures in the ankle joint due to using an implant whose geometry is slightly different from the original talus.

3.5 Conflict of Interest

There are no conflicts of interest to be reported for this publication.

3.6 Funding Source

Funding for this research was provided by Alberta Innovates Technology Futures. Partial funding was provided by NSERC and the University (of Alberta) Hospital Foundation.

3.7 Acknowledgements

We would like to thank Robert Butz, Shannon Hill, and Mason Kim for assisting with this project.

References

Barton, T, F Lintz, and I Winson. "Biomechanical changes associated with the osteoarthritic, arthrodesed, and prosthetic ankle joint." Foot Ankle Surg 17, no. 2 (June 2011): 52-7.

Ferrari, J, DA Hopkinson, and AD Linney. "Size and shape differences between male and female foot bones: is the female foot predisposed to hallux abducto valgus deformity." Journal of the American Podiatric Medical Association 94, no. 5 (2004): 434-52.

Haddad, SL, JC Coetzee, R Estok, K Fahrbach, D Banel, and L Nalysnyk. "Intermediate and long-term outcomes of total ankle arthroplasty and ankle arthrodesis. A systematic review of the literature." J Bone Joint Surg Am 89, no. 9 (September 2007): 1899-905.

Hayes, A, Y Tochigi, and CL Saltzman. "Ankle morphometry on 3D-CT images." The Iowa orthopaedic journal 26 (2006): 1-4.

Hendrickx, RP, SA Stufkens, EE de Bruijn, IN Sierevelt, C van Dijk, and GM Kerkhoffs. "Medium- to long-term outcome of ankle arthrodesis." Foot Ankle Int 32, no. 10 (October 2011): 940-7.

Hintermann, Beat, MD, and Victor, MD Valderrabano. "Total Ankle Replacement." Foot Ankle Clin 8, no. 2 (June 2003): 375-405.

Islam, K, et al. "Three-dimensional geometric analysis of the talus for designing talar prosthetics." Proceedings of the 2014 combined Canadian Orthopaedic Association/American Orthopaedic Association (COA/AOA) and the Canadian Orthopaedic Research Society (CORS) Annual Meeting. Montreal: The Canadian Orthopaedic Association, 2014. 371-8.

Kapandji, AI. The Physiology of the Joints Volume Two The Lower Limb. Toronto: Elsevier, 2011.

Lloyd, John, Sherief Elsayed, Kartik Hariharn, and Hiro Tanaka. "Revisiting the Concept of Talar Shift in Ankle Fractures." Foot Ankle Int 27, no. Oct (October 2006): 793-6.

Mahato, N. "Morphology of sustentaculum tali: Biomechanical importance and correlation with angluar dimensions of the talus." The Foot 21 (2011): 179-83.

Martini, Frederic H., Michael J. Timmons, and Robert B. Tallitsch. Human Anatomy. Fifth. San Francisco: Pearson Education Inc., 2006.

Stagni, R, A Leardini, A Ensini, and A Cappello. "Ankle morphometry evaluated using a new semi automated technique based on X-ray pictures." Clinical biomechanics 20, no. 3 (Mar 2005): 307-11.

Stagni, R, A Leardini, F Catani, and A Cappello. "A new semi-automated measurement technique based on X-ray pictures for ankle morphometry." J Biomech 37, no. 7 (Jul 2004): 1113-8.

Chapter 4 - Finite Element Analysis of a Generic and Custom Talar Prosthetic Compared to a Biological Talus

Abstract

Talar body replacement following talar body collapse is a novel intervention to decrease pain and improve joint mobility. Successful talar body prosthesis depends on understanding the mechanical function of the talus bone. Despite the lack of information on pressures in the ankle, very little research has been performed in this area. The objective of this study was to develop a finite element (FE) model of the ankle to investigate the change in contact pressures and contact areas on the cartilage surfaces surrounding the talus caused by a biological talus, a custom talar implant, and a generic talar implant. The results illustrated that the contact patterns on the surrounding cartilage from the custom implant closely resembled that of the biological talar body, but with higher pressures; and although the contact patterns from the generic implant are slightly different, contact areas and pressures are in general closer to the biological talus than the custom implant. This supports that a generic talar prosthesis may be a suitable implant. This study is the first to demonstrate the incongruency of the talar surface geometry, where the contact occurs at the periphery initially, and transfers to the central region. This phenomenon was seen in both the biological talus and implants. The FE model created was validated by comparing its predictions to cadaveric results from previous studies. This study indicates that a well-designed and appropriately sized generic talus implant closely mimics the original biological talus in terms of contact pressure intensity while the custom implant mimics the contact distribution.

4.1 Introduction

The human skeleton mobilizes in a manner defined by the articulations that connect individual bones. During movement, major joints are load-bearing structures subjected to relatively high magnitudes of load, as high contact forces and compressive loads are transmitted through the joints (Konrath, et al. 1998) (Pena, et al. 2005). Accordingly, the incongruent surface geometry can have a significant effect on the stresses, pressures and pressure gradients inside the tissue (Adeeb, et al. 2004). Most research has focused on the major articulation of the hip, knee and shoulders, with less information produced on the tibia-talar joint in the ankle (D. Anderson, et al. 2006).

The ankle is a complex load-bearing joint, in which the tibia, fibula, and talus articulate with each other. The talus also articulates with the calcaneus via the subtalar joint, as well as the navicular. Due to its location at the near-bottom of the human skeleton, the impact forces on the talus during daily tasks can reach up to 2 to 3 times the body weight (Chi and Schmitt 2005) (Mahato and Murthy 2012). Anderson et al. (2007) completed a validation study for their FE model that assessed pressures on the talus under body weight by assessing the contact that occurred between the tibia and the talus. Predictions of the model were compared to experimental measurements using a Tekscan sensor under 600N of applied axial load. With experimental measurements using two cadaveric ankles, they found that the maximum contact stresses were 3.69MPa and 2.92MPa; the mean contact stresses were 1.96MPa and 1.15MPa; and the contact areas were 295.1mm^2 and 493.6mm^2. Kimizuka et al. (1980) measured the contact area and peak contact pressures on eight amputated ankle specimens under load. They found that under 1000N of load the average contact area was 434mm^2 and the average peak contact pressure was 7.1MPa (ranging from 5-10MPa). Also, the literature has few FE studies that investigated ankle joint mechanics and most of these focused solely on the tibiotalar joint (Cheung, et al. 2005) (Ozen, Sayman and Havitcioglu 2013) (Ozkan, et al. 2013) (Parr, et al. 2013). The high load environment poses a challenge in the mechanical function of the talus body implant after collapse of the talar body as a result of avascular necrosis due to trauma or idiopathic causes (Harnroongroj and Vanadurongwan 1997) (Magnan, Facci and Bartolozzi 2004) (B. Stevens, et al. 2007) (Taniguchi, Takakura and Sugimoto, et al. 2012).

To identify the correct size and geometry for an artificial talus implant, a healthy talus from the opposite ankle can be analyzed as shown by a recent 3D morphometric study that the left and right talus bone of intact human ankle joint have a strong degree of symmetry (K. Islam, et al. 2014a). This knowledge can be used to develop a patient-specific custom talar body implant. More recently, the development of a generic implant with five different sizes has been proposed (K. Islam, et al. 2014b). The 3D geometric analysis showed that after scaling individual talar bodies to a single (average) volume, they can be considered geometrically similar. Also, a proposed range of five implant sizes is shown to be possible for the vast majority of the population (K. Islam, et al. 2014a). Trovato et al. (2016) improved this study by increasing the sample size with 45% of the subjects being female; selectively choosing the implant size, and using incremental jump in the cube root of the volume between sizes. From this analysis, ten unisex implant sizes for the talus bone were created to maintain geometric compatibility of the ankle joint. The current literature however, contains little information regarding the normal mode of contact between the talus and surrounding bones, and that of an implant-cartilage interface.

The purpose of this study is to develop and validate a FE model of the ankle joint that contains the talus and surrounding bones to investigate the contact mode on the cartilage surfaces surrounding the talus when a biological talus, a custom implant (based on the biological talar geometry), and a generic implant are in the ankle mortise. The models are used to investigate the changes in the patterns of the contact distribution and the magnitude of the contact pressures under axial load.

4.2 Materials and Methods

4.2.1 Finite Element Model

Geometry Acquisition

CT scans were taken of the intact right and left cadaveric foot (female; age: 55 years) with the biological talus in the joint in the neutral position. The CT scans were performed using a high-resolution Somatom definition flash scanner with the following specifications: pitch of 0.8mm, gantry tilt of 0 degree, effective mAs of 300, voltage of 80kV, rotation time of 1.0s, slice thickness of 0.6mm, and increment of 0.1mm. The Digital Imaging and Communications in Medicine (DICOM) images were provided with a resolution of 512 x 512 pixels per slide. The DICOM images were imported into a 3D image processing software MIMICS (Materialize NV,

Belgium), where 3D models of each CT scan were digitized into STL file formats. From each of the DICOM image files, separate masks of the distal part of tibia and fibula, talus, navicular bone and calcaneus were created. From the collection of these segmentations, a 3D model of the ankle joint was generated. The STL files were then imported into Geomagic Studio 2013 (Geomagic®, Morrisville, North Carolina; USA), for further image processing.

Implant Selection

In a previous study (Trovato, El-Rich, et al. 2016), we developed a 10-size generic talar body implant that takes into account the gender specific variation. The 3D model (acquired above) was used to determine the volume of the talus (obtained in Geomagic). The volume of the talus was used to select the proper implant size.

Meshing and Pre-Processing

The software HyperMesh (Altair, Troy, Michigan; USA) was used to mesh the geometries. For all bones surrounding the talus, two separate mesh sizes were chosen for the cartilage area and the rest of the bone. The cartilage area on all bone surfaces was meshed with quadrilateral (4-node) elements of an approximate size of 1mm, whereas triangular (3-node) elements with a coarser mesh of up to 2mm were used for the rest of the bone surfaces. The cartilage was built up from the quadrilateral elements to create hexahedron (8-node) elements, by a 3D element offset with a thickness of 1mm. The custom and generic implants were meshed using 1mm triangular elements. To avoid initial surface overclosure due to cartilage creation, the parts were separated until no overlapping of the cartilage surfaces was detected.

The FE model was exported as an Abaqus (Abaqus 6.13, Dassault Systèmes Simulia Corp., Providence; RI, USA) input file. The biological talus, tibia, fibula, calcaneus, navicular, generic and custom implants and cartilage structures were governed by linear elastic material law with properties taken from literature (Table 4-1). Sets of three linear springs (k=20N/mm) located at the position of the anterior and posterior tibiofibular ligaments were added to the model to represent these ligaments (D. D. Anderson, J. K. Goldsworthy, et al. 2007). The cartilage and the corresponding bone elements were bonded together as they shared contact nodes at the surface (Figure 4-1).

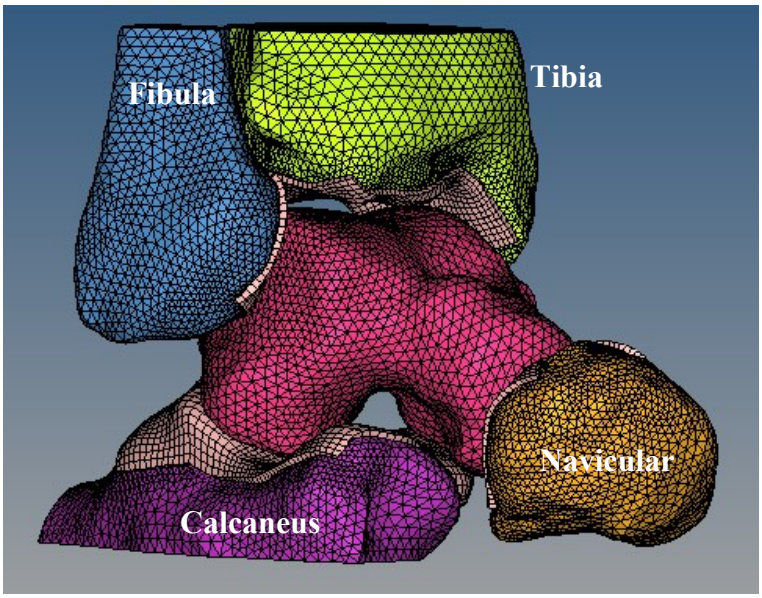

Figure 4-1: Mesh of the finite element model

Table 4-1: Assigned material properties in the FEA model

	E Young's Modulus (MPa)	Poisson's ratio
Bone	20,000 (Elias, et al. 2008) (Nigg and Herzog 1999)	0.3 (Parr, et al. 2013)
Implants – Titanium	119,000 (Elias, et al. 2008) (Karacali 2015)	0.32 (Karacali 2015)
Cartilage	12 (D. D. Anderson, J. K. Goldsworthy, et al. 2007)	0.42 (D. D. Anderson, J. K. Goldsworthy, et al. 2007)

Using kinematic coupling, the proximal tibia and fibula surfaces, and the joint back surfaces of the calcaneus and navicular were constrained to their own respective reference points to control the displacements, boundary conditions, and loading conditions of each bone.

A compressive load of 2000N was applied on the tibia and fibula in 3 consecutive static general time steps: (1) the model was brought to the contact state while the talus was fixed; (2) the talus bone was allowed to adjust freely without any constraints, while the surrounding bones remained fixed in place; (3) loads were applied incrementally to the tibia and fibula reference point until the overall load reached 2000N while the tibia and fibula displacements were unrestrained. For steps 1 and 2, a displacement-controlled manner was employed to control displacement. The tibia and fibula were brought down distally to come into contact with the talus while the

calcaneus and navicular was displaced up and posteriorly respectively to contact the talus/implant. In the final step, a force control approach was defined wherein the load was applied to the tibia and fibula. The general contact assignment was used with balanced contact definitions for the biological case (cartilage coming into contact with cartilage) and surface-to-surface contact assignment was used for master-slave contact definition for the implant cases (where the implant – master, comes into contact with the cartilage – slave). The tangential contact behaviour was defined by the penalty method with a friction coefficient of 0.002 (Adeeb, et al. 2004), whereas the normal contact behaviour was defined as hard contact.

4.3 Validation Model

The biological talus, tibia and fibula construct of the current model were used for validation. A compressive load was applied on the tibia and fibula construct while the talus was kept fixed to mimic the loading scenario and boundary conditions used in the FE and experimental studies of Anderson et al (2007) to best compare results. The contact area, peak contact pressure (PCP) and mean contact pressure (mean CP) on the surrounding tibia articular cartilage were predicted and determined and compared to results of Anderson et al (2007). The values under 600N and 1000N load were compared to results reported in Figure 4-2.

4.4 Comparison of Implant Performance

The mode of contact between the talus and the surrounding articular cartilage under 2000N load was investigated for four different cases of tali:

- Case 1 (*Biological*): the biological talus with articular cartilage
- Case 2 (*Custom Implant*): the custom implant with the same volume and geometry as Case 1, but modelled as titanium
- Case 3 (*Generic Implant*): the generic implant modelled as titanium
- Case 4 (*Generic (N - New Fibula Location)*): the exact same as Case 3 but with the fibula translated 1mm (medially) closer to the tibia as the tibia can translate 1-3mm (Scott, et al. 2007). Case 4 is defined to ensure that contact is made between the implant and the fibula.

The contact pressure distribution in the surrounding articular cartilage under different axial loads (1000N and 2000N), the contact area, PCP and mean CP were analyzed on the cartilage surfaces throughout all steps of the loading phase. The mean CP was calculated by exporting magnitudes of contact pressure of all surface nodes into an Excel table and averaging the non-zero values.

4.5 Results

4.5.1 Implant Selection

Based on the measured volume of the subject's contralateral talus (30,034mm^3), implant body size number 4 (size range of 28,906mm^3 to 32,964mm^3) was chosen based on our previous research (Trovato, El-Rich, et al. 2016).

4.5.2 Finite Element Model

Validation Results

The contact area, PCPs and mean CPs on the tibia when in contact with the biological talus are presented alongside the cadaveric values from Anderson et al (2007) and Kimizuka et al (1980) in Figure 4-2.

Figure 4-2: Contact pressures and areas of the validation model and cadaveric specimens

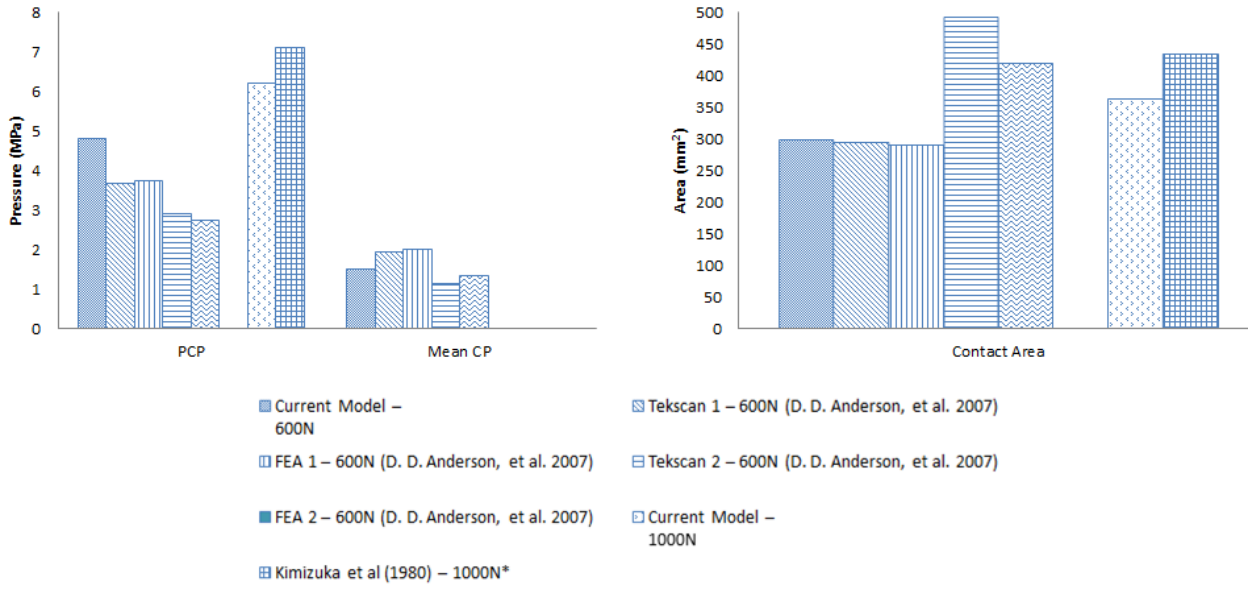

Implant Performance

The tibia, fibula, navicular, and calcaneus cartilage when they come into contact with the biological talus and implants are shown at 1000N and 2000N of applied load (Figure 4-3). The contact is shown on the surrounding cartilage only as opposed to the talus itself because the implants are not biological material. Additionally, it is easier to isolate the different areas of

contact on each of the bones by focusing on the specific areas of articular cartilage. Areas of high pressure (red) can be regarded as areas of contact, and areas of low pressure (blue) are areas with no contact. The results show almost identical patterns between the biological talus and the custom implant on all four surfaces; however with higher pressures caused by the custom implant. The results showed similar patterns between the biological talus and the generic implant on the tibia, fibula and calcaneus; however the location of the contact on the navicular surface was in a different location. The contact pressures caused by the generic implant appeared similar to that of the biological talus. In all cases the contact on the tibia shows contact starting only at the peripheral (medial and lateral regions) of the talar dome with the lower axial load of 1000N and as the axial load increases to 2000N, the contact areas enlarge, as well as development of contact at the central regions is beginning to occur.

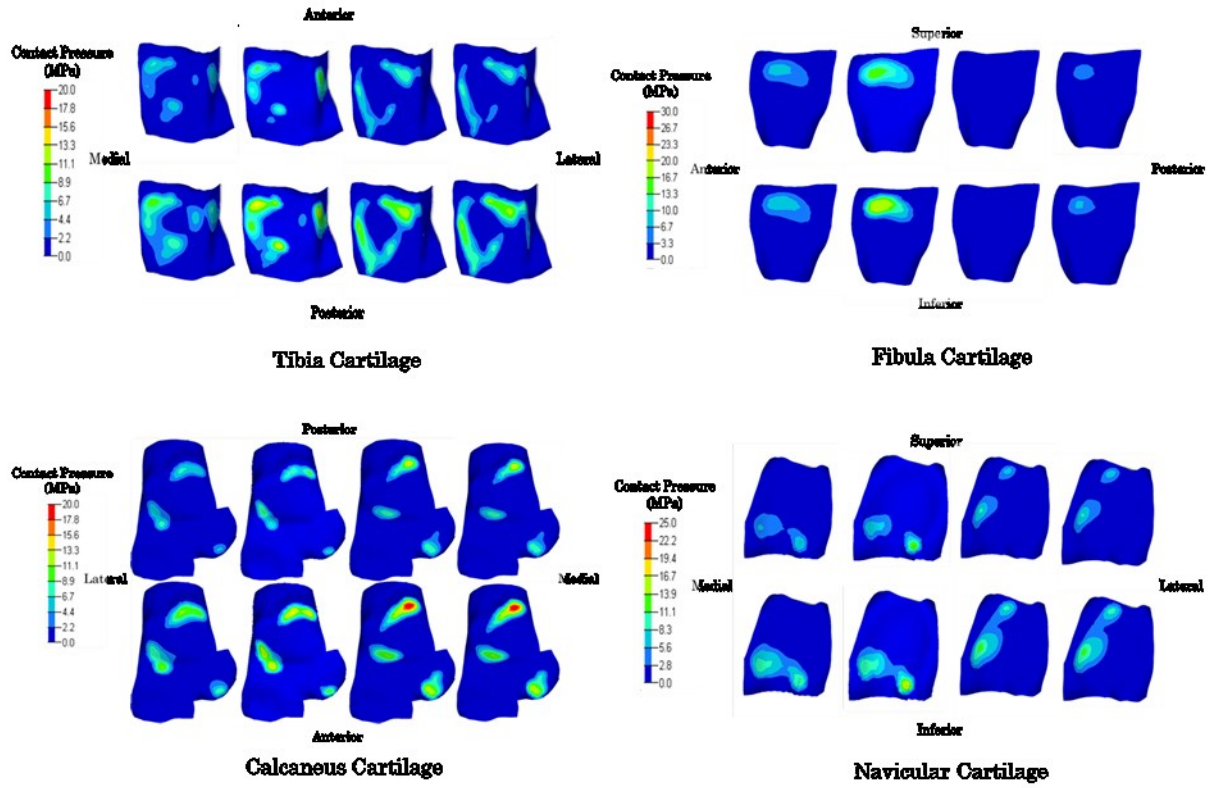

Figure 4-3: Contact distribution of cartilage surfaces; for each surface: under 1000N (top) and 2000N (bottom) – from left to right biological, custom, generic, generic (N)

A sagittal cross section of the joint illustrates the congruency profile of the joint surfaces when the biological talus and implants are in contact at 2000N of load (Figure 4-4).

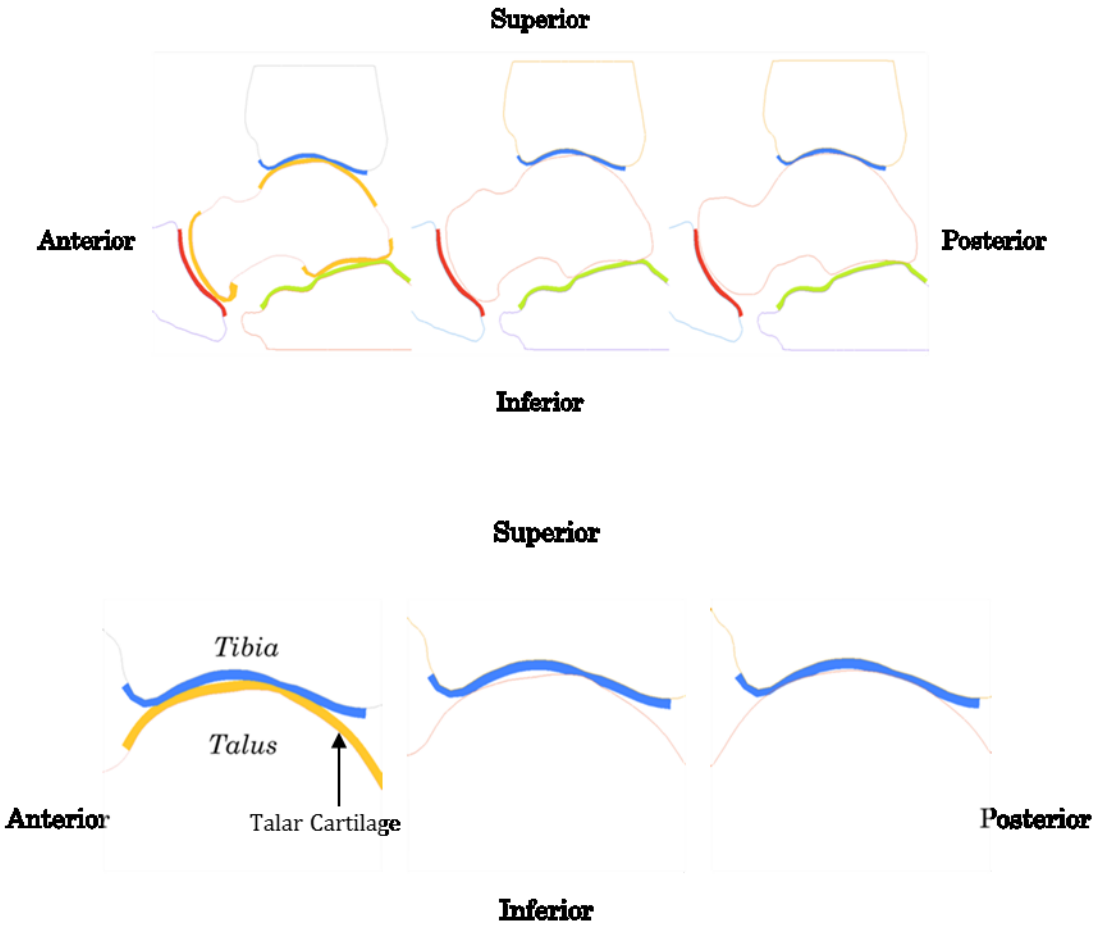

Figure 4-4: Cross section and close-up cross section of the joint illustrating contact differences – from left to right biological, custom, generic

The contact area, PCPs and mean CPs on the tibia, fibula, calcaneus and navicular articular cartilage when in contact with the biological talus and implants are plotted versus load magnitude in Figure 4-5, Figure 4-6, Figure 4-7, and Figure 4-8 respectively. The biological talus had the highest contact areas and lowest contact pressures on all of the cartilage surfaces with the exception of the fibula. For the tibia and navicular cartilage, the contact area and contact pressures caused by the generic implant were closer to the biological talus than the custom implant. For the fibula, the custom implant had the largest contact pressures and the generic implant had the lowest contact pressures and contact area (with the generic implant from Case 3 having zero contact area and zero pressure). On the calcaneus, the custom implant had slightly closer PCPs to the biological talus; however, the contact area and mean CP from the custom implant was almost identical to the generic implant.

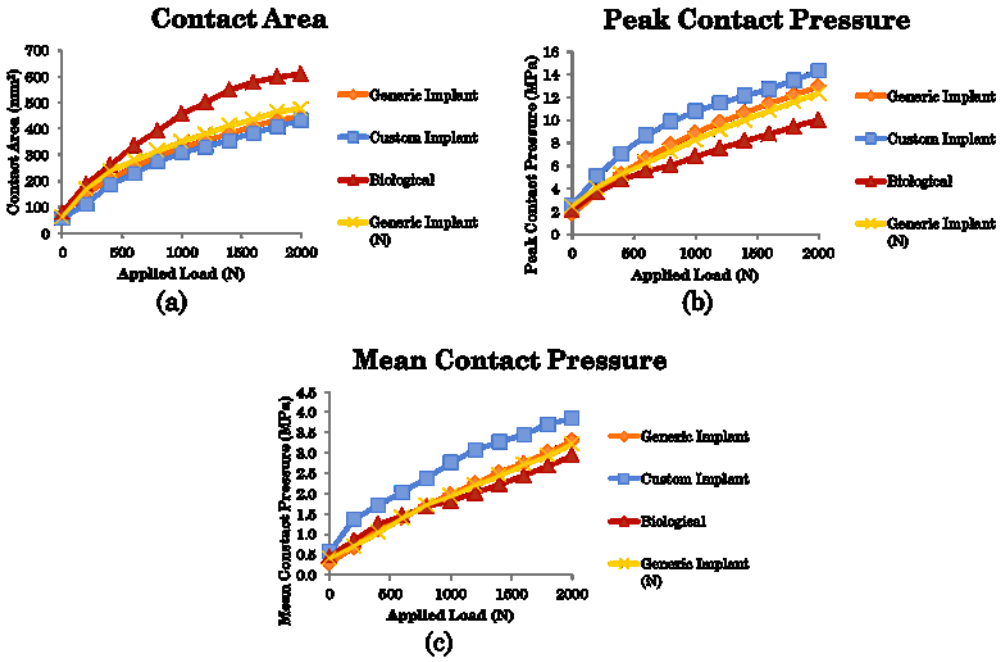

Figure 4-5: Tibia cartilage (a) contact area, (b) peak contact pressure, and (c) mean contact pressure

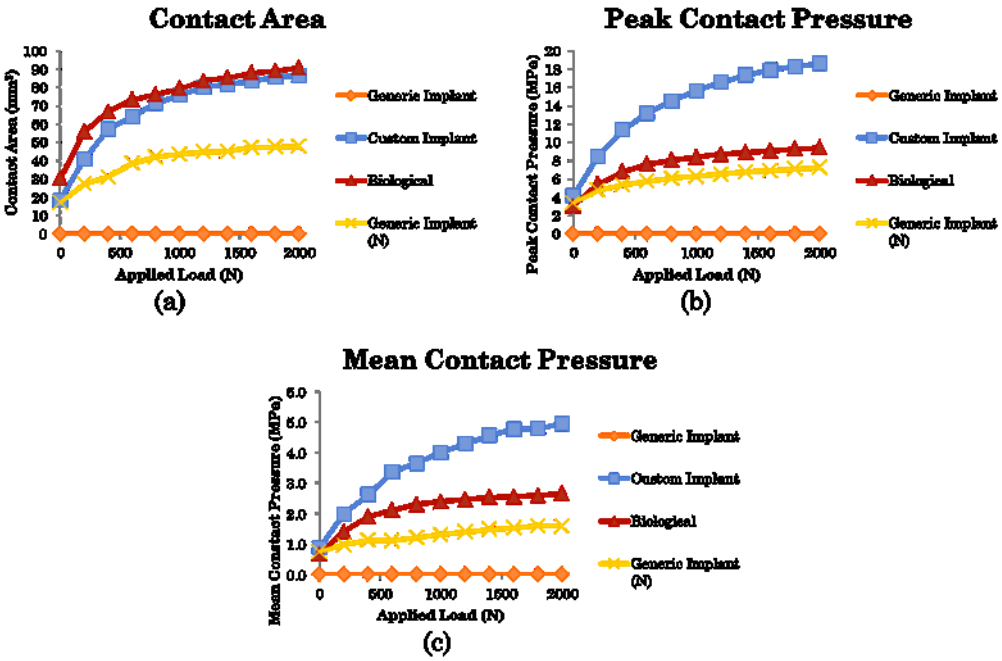

Figure 4-6: Fibula cartilage (a) contact area, (b) peak contact pressure, and (c) mean contact pressure

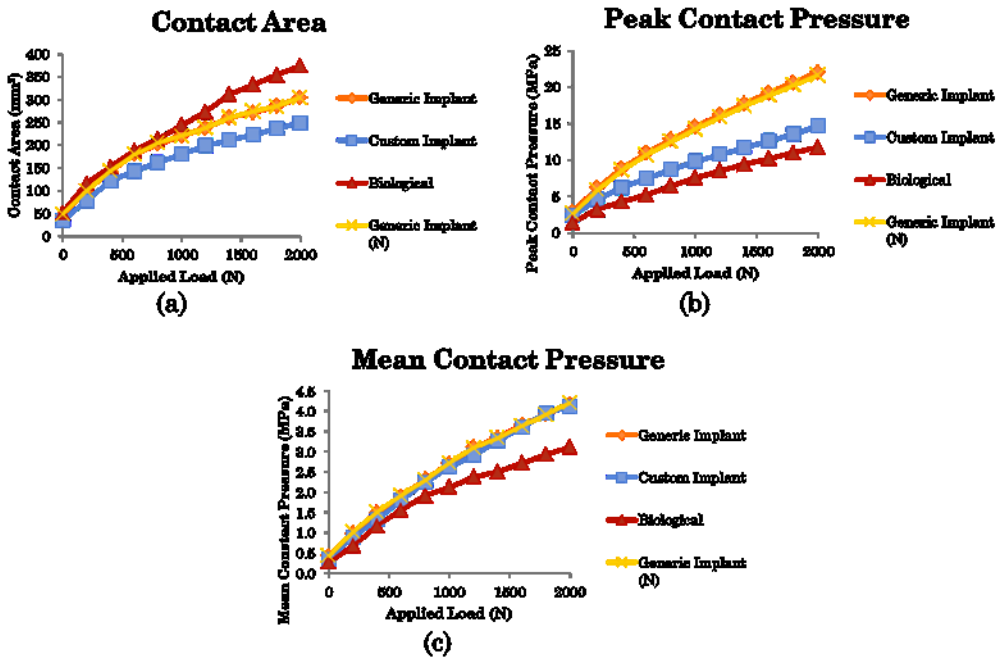

Figure 4-7: Calcaneus cartilage (a) contact area, (b) peak contact pressure, and (c) mean contact pressure

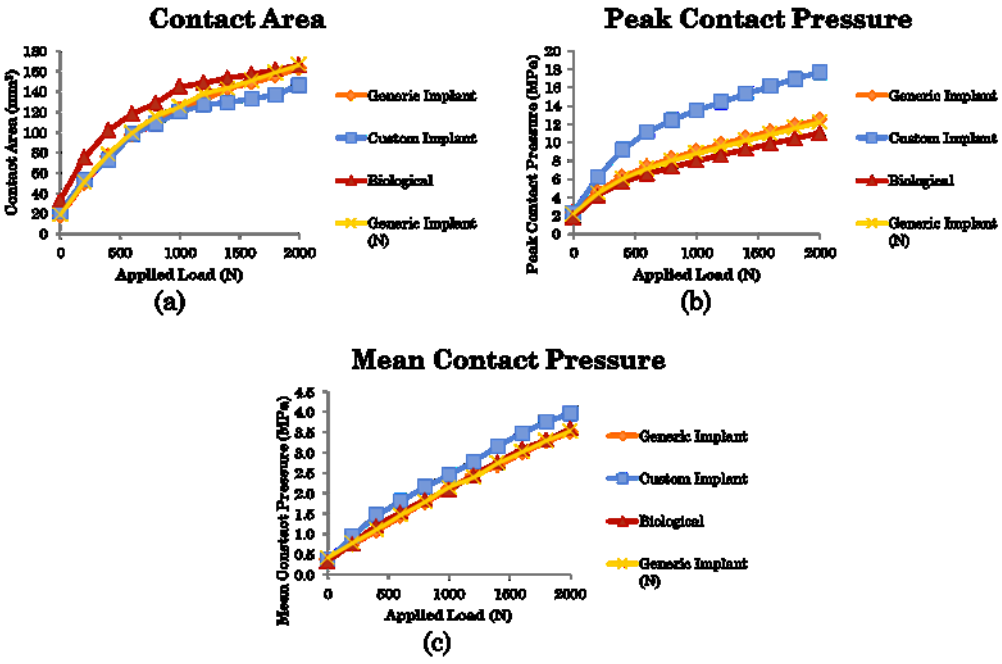

Figure 4-8: Navicular cartilage (a) contact area, (b) peak contact pressure, and (c) mean contact pressure

4.6 Discussion

Talus bone replacement decreases pain and improves mobility in a case of talar body collapse (Taniguchi et al. 2015). Development of a generic talar body prosthesis depends on an improved understanding of the morphometric and geometric shape of the talus bone (K. Islam, et al. 2014a). A recent study has proposed the use of a generic "off-the-shelf" talus implant rather than a patient-specific implant to replace the talus (Trovato, El-Rich, et al. 2016). The current study compared the contact mechanism on the surrounding cartilage under compressive load and investigated effects of the geometric and material variations between a biological talus with a custom implant and a generic implant.

Very few FE studies of the ankle joint exist in the literature. There have been reports of models that simulate the patient's whole leg with tibia vara (Ozkan, et al. 2013), concentrate on the contact pressure on the sole of the foot (Cheung, et al. 2005), or investigate the peak pressure in the ankle joint by simulating the distal tibia (without fibula) and the talus (D. D. Anderson et al. 2007). Predictions of the developed FE model in terms of contact area and pressure in the talar-tibia joint were in good agreement with the limited data reported in the literature. The contact areas at 600N and 1000N fell within the range found by Anderson et al (2007) (295mm^2 to 493mm^2); and Kimizuka et al (1980) (354mm^2 to 550mm^2), respectively. Although the PCP at 600N was higher than found in the Anderson et al. (2007) study, the mean CP was well within the range they found (1.15MPa to 2.02MPa). The higher PCP is likely attributed to the difference in geometry. Kimizuka et al (1980) did not measure the mean CP but found that the average PCP among the 8 subjects was 7.1MPa with a range of 5MPa-10MPa at 1000N of applied load. Our model's predicted PCP that fell within that range. The cartilage was modeled with a uniform thickness of 1mm due to large discrepancies between reported values (Millington, et al. 2007). The load of 2000N was chosen because impact forces on the talus during daily tasks can reach up to 2 to 3 times the body weight (Chi and Schmitt 2005) (Mahato and Murthy 2012).

The contact patterns on the tibia cartilage predicted in this study (Figure 4-3) clearly showed that contact initially occurred at the periphery, and as the axial loading increased, additional pressures were transferred to the central region, which agrees with findings of Adeeb at el. (2004) (who showed that in major diarthrodial joints such as the knee, the hip and the shoulder, contact

initiates at the periphery, and moves towards the center with increasing load). The results of the biological talus analysis support that the contact mode is similar in the ankle joint.

This study investigated the changes in contact distribution between a biological talus, a custom implant and a generic implant in the neutral position during loading up to 2000N. The contact distribution patterns showed good conformity between the biological talus and the custom implant; however, the peak and mean contact pressures caused by the custom implant were higher than the biological talus on all surrounding articulating surfaces. This correlates with the contact areas caused by the custom implant being slightly lower than that of the biological talus and the implant being made out of titanium. This is likely due to the fact that the custom implant had the same size and geometry as the biological talus but made of harder material (titanium) and had no cartilage which prevented the contact area from increasing as load was applied; as opposed to when both surfaces had cartilage and were able to deform and come into increased contact with each other. The contact distribution patterns between the generic implant and the biological talus were similar in all cases with the exception of the navicular surface which is less problematic as the navicular is not a load bearing joint and has greater ability to adjust position in the clinical scenario. The generic implant contact areas, PCPs and mean CPs were closer to the biological talus than the custom implant with the exception of the calcaneus (where the PCP was only slightly higher on the generic implant over the custom implant and the mean CP was similar to the custom implant) and the contact on the fibula (which was non-existent for case 3 and very low for case 4). This indicates that generally, the generic implant may provide equal or better results than a custom implant for patients as it appears to cause contact pressures closer to the range one experiences with a biological talus. This could be due to the fact that because the generic implant is slightly different than the custom implant, it is able to adjust to a more amiable position in the joint; whereas the custom implant has less space to adjust. In this case, the volume of the generic implant was very similar to the volume of the custom implant (33,587mm^2 compared to 33,013mm^2); as such, the difference cannot be attributed to the volume. An additional possibility is that the lateral and medial shoulders of the talus bone are slightly more pronounced at the central and anterior locations. This could cause extra pressures on the tibial plafond as the implant is more flat and as such, able to distribute the load more uniformly which is illustrated in Figure 4-5 which shows the contact area of the custom implant to be much lower than the biological talus or generic implant.

One area of concern for the custom implant could be the lack of pressure caused by the gap between the custom implant and the fibula as the fibula has a role in ankle stability (Goh, et al. 1992). However, there may be some adjustment of the fibula relative to the tibia in in-vivo conditions, as it has been shown that the tibiofibular joint may translate 1-3mm in a range of loading conditions (Scott, et al. 2007); and the positions of the bone were based on the biological talus being in the joint. As such, it is possible that there will be contact between the fibula and custom implant as shown by case 4, wherein the fibula was brought 1mm closer to the tibia. This indicates that a well-defined and appropriately sized generic talar implant would display more similar contact pressures and areas as the biological talus, as opposed to the custom implant. The results support the methodology proposed by Islam et al. (2014) and Trovato et al. (2016) in which generic talus geometries can be used and the size can be chosen based on the volume of the contralateral talus of the same patient. However, the cartilage thickness and cartilage properties could be more thoroughly investigated by incorporating MRI data. The objective of our paper was to investigate if a generic implant could be used instead of custom implant. The results were surprising in that the generic implant in our case showed equal or better pressure redistribution than the custom implant.

A limitation of this study is the modeling of the cartilage, where there exists discrepancy within the literature regarding the material properties for the articulating cartilage in the ankle joint. This study focused on the instantaneous loading of the joint and as such, modelled the material properties as a linear elastic equivalent for instantaneous loading. These discrepancies could lead to different values for the contact pressures; however, because the model was validated using cadaveric values for pressure, the results of this study should have accurate results regarding the pressures. Additionally, this study focuses on the comparison of the different cases of tali in the joint so the most important consideration was for the cartilage properties to be consistent between the models which it was. Modeling the cartilage by a simple element offset layer is an additional limitation. With this approach, the cartilage has the same thickness over the whole area, which only roughly mimics the real situation. Also, in this study the navicular bone and the calcaneus bone are fixed in place when in reality, there is some movement allowed.

4.7 Conflict of Interest

There are no conflicts of interest to be reported for this publication.

4.8 Funding Source

Funding for this research was provided by Alberta Innovates Technology Futures and NSERC.

4.9 Acknowledgements

We would like to thank Behzad Vafaeian and Sadegh Naserkhaki at the University of Alberta for assistance with the Abaqus software.

References

Adeeb, Samer, Ezzeldin Y. Sayed Ahmed, John Matyas, David A. Hart, and Cyril B. Frank. "Congruency effects on load bearing in diarthrodial joints." Computer Methods in Biomechanics and Biomedical Engineering 7, no. 3 (2004): 147-157.

Anderson, Donald D., et al. "Intra-articular contact stress distributions at the ankle throughout stance phase--patient-specific finite element analysis as a metric of degeneration propensity." Biomech Model Mechanobiol. 5, no. 2-3 (2006): 82-89.

Anderson, Donald D., Jane K. Goldsworthy, Wendy Li, M. James Rudert, Yuki Tochigi, and Thomas D. Brown. "Physical validation of a patient-specific contact finite element model of the ankle." Journal of Biomechanics, 2007: 1662-1669.

Cheung, Jason Tak Man, Ming Zhang, Aaron Kam-Lun Leung, and Yu-Bo Fan. "Three-dimensional finite element analysis of the foot during standing--a material sensitivity study." Journal of Biomechanics 38 (2005): 1045-1054.

Chi, Kai Jung, and Daniel Schmitt. "Mechanical energy and effective foot mass during impact loading of walking and running." Journal of Biomechanics 38 (2005): 1387-1395.

Elias, C.N, J.H.C. Lima, R. Valiev, and M.A. Meyers. "Biomedical Applications of Titanium and its Alloys." Journal of Materials, 2008: 46-49.

Goh, James, Joo Ang, Philippe Bayon, and Robert Pho. "Biomechanical Study on the Load-Bearing Characteristics of the Fibula and the Effects of Fiblar Resection." Clinical Orthopaedics and Related Research, no. 279 (1992): 223-8.

Harnroongroj, T., and V. Vanadurongwan. "The talar body prosthesis." Journal of Bone and Joint Surgery 79 (1997): 1312-1322.

Islam, K, et al. "Three-dimensional geometric analysis of the talus for designing talar prosthetics." Proceedings of the 2014 combined Canadian Orthopaedic Association/American Orthopaedic Association (COA/AOA) and the Canadian Orthopaedic Research Society (CORS) Annual Meeting. Montreal: The Canadian Orthopaedic Association, 2014. 371-8.

Islam, K., et al. "Symmetry analysis of talus bone: A Geometric morphometric approach." Bone and Joint Research 3, no. 5 (2014): 139-145.

Islam, Kamrul, et al. "Three-dimensional geometric analysis of the talus for designing talar prosthetics." Journal of Engineering in Medicine 228, no. 4 (2014): 371-378.

Karacali, O. "Fatigue Analysis of Ti-55 Alloy Material for Multifunctional Surgical Instruments in Medical Engineering." 4th International Congress APMA. Fethiye, 2015. 1199-1201.

Kimizuka, Mamori, and Hisashi, Fukubayyashi, Toru Kurosawa. "Load-bearing Pattern of the Ankle Joint." Archives of Orthopaedic and Trauma Surgery, 1980: 45-49.

Konrath, Gregory A., Andrew J. Hamel, Steve A. Olson, Brian Bay, and Neil A. Sharkey. "The role of the acetabular labrum and the transverse acetabular ligament in load transmission in the hip." The Journal of Bone and Joint Surgery 80-A, no. 12 (1998): 1781-1788.

Magnan, Bruno, Elisa Facci, and Pietro Bartolozzi. "Traumatic loss of the talus treated with a talar body prosthesis and total ankle arthroplasty. A case report." The Journal of Bone and Joint Surgery 86-A, no. 8 (2004): 1778-1782.

Mahato, Niladri Kumar, and Sathiya Narayana Murthy. "Articular and angular dimensions of the talus: inter-relationship and biomechanical significance." The Foot 22 (2012): 85-89.

Millington, S.A., M. Grabner, R. Wozelka, D.D. Anderson, S.R. Hurwitz, and J.R. Crandall. "Quantification of ankle articular cartilage topography and thickness using a high resolution stereophotography system." OsteoArthritis and Cartilage, 2007: 205-211.

Nigg, Benno, and Walter Herzog. Biomechanics of the Musculo-skeletal System. Baffins Lane, Chichester: John Wile & Sons Ltd, 1999.

Ozen, Mustafa, Onur Sayman, and Hasan Havitcioglu. "Modeling and stress analyses of a normal foot-ankle and a prosthetic foot-ankle complex." Acta of Bioengineering and Biomechanics 15, no. 3 (2013): 19-27.

Ozkan, Arif, Halil Atmaca, Ibrahim Mutlu, Talip Celik, Levent Ugur, and Yasin Kisioglu. "Stress distribution comparisons of foot bones in patient with tibia vara: a finite element study." Acta of Bioengineering and Biomechanics 15, no. 4 (2013): 67-72.

Parr, W. C. H, U. Chamoli, A. Jones, W. R. Walsh, and S. Wroe. "Finite element micro-modelling of a human ankle bone reveals the importance of the trabecular network to mechanical performance: new methods for the generation and comparison of 3D models." Journal of Biomechanics 46 (2013): 200-205.

Pena, E., B. Calvo, M.A. Martinez, and M. Doblare. "A three-dimensional finite element analysis of the combined behavior of ligaments and menisci in the healthy human knee joint." Journal of Biomechanics 39 (April 2005): 1686-1701.

Scott, Jacob, Ho Lee, Wael Barsoum, and Antonie J van den Bogert. "The effect of tibiofemoral loading on proximal tibiofibular joint motion." Journal of Anatomy 211, no. 5 (2007): 647-53.

Stevens, B. W., C. M. Dolan, J. G. Anderson, and C. D. Bukrey. "Custom talar prosthesis after open talar extrusion in a pediatric patient." Foot Ankle International 28, no. 8 (2007): 933-938.

Taniguchi, A., et al. "An Alumina Ceramic Total Talar Prosthesis for Osteonecrosis of the Talus." J Bone Joint Surg Am, no. 97 (2015): 1348-53.

Taniguchi, A., et al. "The use of a ceramic talar body prosthesis in patients with aseptic necrosis of the talus." The Journal of Bone and Joint Surgery 94-B, no. 11 (2012): 1529-1533.

Trovato, A, M El-Rich, S Adeeb, and N Johma. 2016. "Geometric Analysis of the Talus and Development of a Generic Talar Prosthetic." *Foot and Ankle Surgery* Manuscript FAS-D-16-00068.

Chapter 5 - Analysis of a Generic Talar Prosthetic with a Biological Talus: A Cadaver Study

Abstract

Despite advances in the evolution of ankle prosthetics, maintaining full ankle joint function after a talar injury remains a challenge. In a previous study we created a unisex implant in ten sizes for the talus bone to maintain geometric compatibility of the ankle joint. This study evaluates the feasibility of using the implants using cadaveric assessment and finite element analysis (FEA). Ten cadavers were used in this study and the left ankle from each cadaver was scanned with computed tomography and modeled to determine which implant size would be used for the right talus. This was done to mimic a clinical setting where the right ankle would be too damaged to accurately determine size. The implants were 3D printed and the right ankles were scanned with the biological talus and again with the implant inserted in place of the biological talus. Three-dimensional geometry of the ankle joint was reconstructed from CT-scan data and the location of the implant within the ankle joint was compared to the location of the biological talus when the surrounding bones from each scan were aligned with each other. The averages among specimens' positive and negative average-deviations were 0.91mm and 0.70mm respectively. Seventy percent of the deviations on the talar dome between the biological talus and implant were within an acceptable range. The deviations had a direct correlation with the contact areas caused by a 2000N axial load determined through FEA. Results showed that there would not be excessive contact pressures caused by a generic implant. This study yields promising results to support the use of a generic talus bone prosthetic.

5.1 Introduction

After calcaneus fractures, talus fractures are the most frequent of all tarsal bone fractures and account for 0.1-0.85% of all fractures (Bhandari and Adili 2011) (Huang and Cheng 2005) (Santavirta, et al. 1984). They are most common in a young, active patient population and are more likely to occur in men than in women by a ratio of three to one (Bhandari and Adili 2011) (Thordarson 2007). Fractures of the talar neck, which account for approximately 50% of significant injuries to the talus (Thordarson 2007), can result in avascular necrosis (AVN) in 20-100% of patients with displaced fractures. The avascular bone can be unsuitable to hold the required load and collapse can occur resulting in severe incongruity of the ankle joint and in turn, pain, swelling, and restricted motion.

The most common surgical option in caring for this injury is ankle arthrodesis (fusion), wherein talus is fused to the tibia or the tibia and calcaneus. Although arthrodesis often enables the patient to walk with decreased pain, it results in loss of motion and function of the joint (Barton, Lintz and Winson 2011) (Haddad, et al. 2007). Additionally, this procedure can be difficult because of a lack of healthy bone due to AVN.

Ankle arthroplasties have become a more desirable alternative to fusion as they have the potential to offer increased mobility of the ankle joint. More recently, they have been designed and implanted with increasing success (Kakkar and Siddique 2011); however, these ankle arthroplasties are not suitable when the talus fracture results in AVN because the talus is often lacking in healthy bone stock that is required for talar fixation of the prosthesis.

An appropriate solution to the issues associated with arthrodesis and arthroplasties is a talar body implant that replaces the avascular portion of the talus or the entire talus to maintain full ankle joint function. At this time, there have been some reports of talar body replacements. All implants have been custom made from various materials - stainless steel (Harnroongroj and Vanadurongwan 1997), alumina ceramic (Tanaka, et al. 2003) (Taniguchi, Takakura and Tanaka, et al. 2015), titanium alloy (Magnan, Facci and Bartolozzi 2004), and cobalt-chrome (B. W. Stevens, et al. 2007). The prostheses developed by Harnroongroj and Vanadurongwan used custom measurements of volume and dimensions (including curvatures) of the contralateral talus; they were implanted in 16 patients. Tanaka et al. (2003) developed a prosthesis similar to

Harnroongroj and Vanadurongwan (1997) and implanted it in three patients. Both Magnan et al. (2004) and Stevens et al. (2007) replaced a talus utilizing CT scans to develop a prosthesis based on the real geometry of the bone. All of these implants were custom-made and as such, involve increased time between injury and surgery and can be expensive.

The next step in the field of talus bone prosthetics would be to develop a generic talus bone prosthetic in different sizes to mitigate the costs and the extended time between onset of injury and surgery. This requires a generalization of the geometry of the talus. Islam et al. (2014) proposed an implant in five sizes; however, that study had limitations including lack of a diverse sample selection such that the female population was vastly underrepresented, a randomly selected implant, and an incremental jump in size of volume (which will be more significant in the smaller sizes as the volume is a cubic function). Trovato et al. (2016) improved upon this study by increasing the sample size with 45% of the subjects being female, selectively choosing the implant size, and using incremental jump in the cube root of the volume between sizes. From this analysis, ten unisex implant sizes for the talus bone were created to maintain geometric compatibility of the ankle joint.

Trovato et al. (2016) created a finite element model to test the validity of using a generic implant in lieu of a custom made implant. The model of the joint was in the neutral position complete with the bones surrounding the talus (tibia, fibula, calcaneus and navicular including cartilage) and was analyzed with the biological talus (with cartilage), the generic implant, or the custom implant (based off the biological geometry) in the ankle joint. The contact pressures and areas on the cartilage surfaces of the tibia, fibula, calcaneus and navicular, as well as on the implant itself were obtained under axial load to determine the impact of using a generic or a custom implant. It was determined that the contact pressures and areas were closer to the biological talus when using the generic implant over the custom implant, and as such, a custom implant may not be a superior solution to a generic implant.

This study evaluates the feasibility of using 10 implant sizes by verifying the joint compatibility of the talar implants using cadaveric assessment; and attempts to link the pressure distribution and contact area differences between the biological and generic implant to deviations in geometry between the two implants when situated in the cadaveric ankle. To achieve this, we

explored how a generic talar implant fits into the ankle joint as compared to the biological talus using cadaveric assessment and FEA.

5.2 Materials and Methods

5.2.1 Experimental Technique

Ankle Joint Imaging

After obtaining ethical approval from the University of Alberta research ethics board, 10 cadavers (4 male, 6 female; age at death 84.5±12.0 years) were obtained from the University of Alberta's Anatomy department. The feet were isolated from the cadavers approximately 100mm above the ankle joint and a CT scan was performed on the left ankle. The implant size for the talus was selected from the scan of the contralateral talus (in this case, the left talus) because in clinical practice, the talus being replaced is damaged and as such, is not reliable to determine the original size of the talus.

Each ankle was placed in the CT scanner approximating the clinical position. The CT scan was performed using a high-resolution Somatom definition flash scanner with the following specifications: pitch 0.8mm, gantry tilt 0 degree, effective mAs 300, voltage 80kV, rotation time 1.0s, a constant slice thickness of 0.6mm and increment of 0.1mm. The Digital Imaging and Communications in Medicine (DICOM) images were provided with a resolution of 512 x 512 pixels/slide.

Geometric Analysis

From these scans, the DICOM images were imported into the 3D image processing software, MIMICS (Materialize NV, Belgium), and a 3D model was created (Figure 5-1). Following this, the computer software Geomagic (Geomagic®, Morrisville, North Carolina; USA) was used to obtain the volume of the talus and from this volume, the implant size for the right talus was selected by comparing the volume of the talus to the implant sizes defined in a previous study (Trovato, El-Rich, et al. 2016). The talus was then scaled up by 0.5mm over the entire surface area to account for articular cartilage.

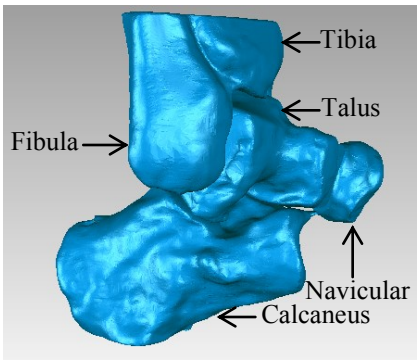

Figure 5-1: 3D model of talus and surrounding bone

The biologic talus was surgically removed from the ankle by severing surrounding ligaments. Elastic bands were placed around the ankle to maintain some connectivity (Figure 5-2).

Figure 5-2: Cadaveric foot with elastics

The biologic talus was inserted back into the right ankle and was coronally scanned three times: (1) in a neutral position (0˚), (2) 20˚ dorsiflexion, and (3) 20˚ plantarflexion. Subsequently, the biologic talus was removed from the ankle and replaced by the prosthetic implant. The implant in the ankle was scanned using the same procedure as the scan of the biologic talus. Three dimensional models of the scans were reconstructed in the same manner as stated above. A custom holder, (Figure 5-3), was used to hold the foot in the correct position.

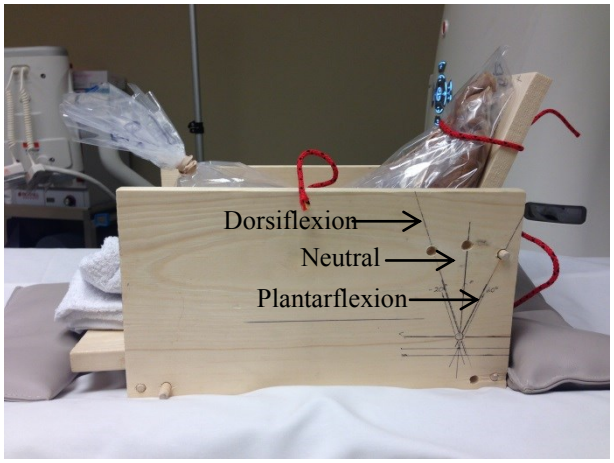

Figure 5-3: Cadaver foot holder

5.2.2 Implant vs. Biological Talus: Geometric Comparison

For each angle and each specimen, the position of the Talus-Tibia and Fibula (TTF) articulating surfaces was compared between the biologic and the implant tali. The articulating surface was isolated and the change of position of the implant was appraised by comparing the talar dome surface of the biological talus and the implant using the following five steps.

1. All bones, except for the talus, tibia, and fibula were deleted.
2. The tibia and fibula from the model with the biological talus and talar implant were aligned to the each other.
3. The model was cropped to facilitate viewing of the articulating surfaces. The tibia and fibula were cropped approximately 20mm above the highest point on the talus. The tali in both models were cropped off to focus on the articulating talar dome (Figure 5-4).
4. The tibia and fibula were re-aligned after cropping.
5. The deviation in the talar dome of the biological talus and the implant was examined.

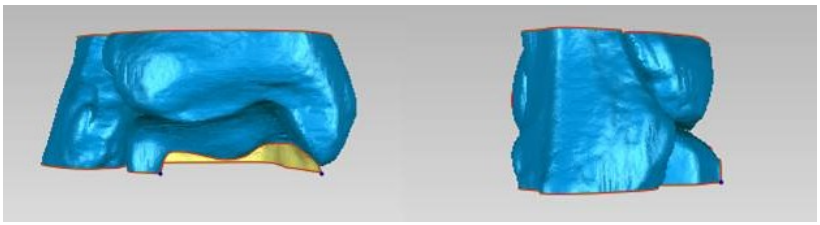

Figure 5-4: Neutral biological tibia, fibula and talus cropped anterior and lateral view

This alignment and the deviation analysis were carried out using Geomagic. The alignment of the tibia and fibula was achieved using the Geomagic software built-in best-fit approach. The relative positions of the biological talus and implant relative to the tibia and fibula from the biological and implant scans were kept fixed. Once the models were aligned, the tibia and fibula on each model were deleted leaving only the talus and the implant. Deviation contour maps (DCMs) between the biological talus and implant were generated using the Geomagic 3D Compare Analysis. This resulted in finding the relative difference between the surfaces of the biological talus and the implant in the three defined positions.

5.2.3 Implant vs. Biological Talus: Finite Element Comparison

The ankle joint of subject 4 used in this cadaveric study was modeled in a different study (Trovato et al., 2016). The model of the right foot included the tibia, fibula, calcaneus and navicular (along with 1mm of cartilage on the surfaces that articulate with the talus). There were two models for the talus bone itself; the first being the biological bone (scaled up by 0.5mm all around to account for some cartilage that was not detected by the CT scan and modelled as titanium) and the second being a generic implant developed by Trovato et al (2016), also modelled as titanium.

The models were created by importing the DICOM images obtained from CT scans into MIMICS where 3D models of each CT scan were digitized into STL file formats. STL files were then imported into Geomagic Studio, where it was utilized for further image processing. HyperMesh (Altair, Troy, Michigan; USA) was used to mesh the geometries. The cartilage surfaces on all bone was defined as quadrilateral elements and meshed with an approximate size of 1mm, whereas triangular elements with a coarser mesh of up to 2mm were used for the rest of the bone. The cartilage was built up from the quad elements to create hexahedron elements, by a

3D element offset with a thickness of 1mm. The biological and generic implants were meshed using a 1mm triangular mesh. The mesh is illustrated below in Figure 5-5.

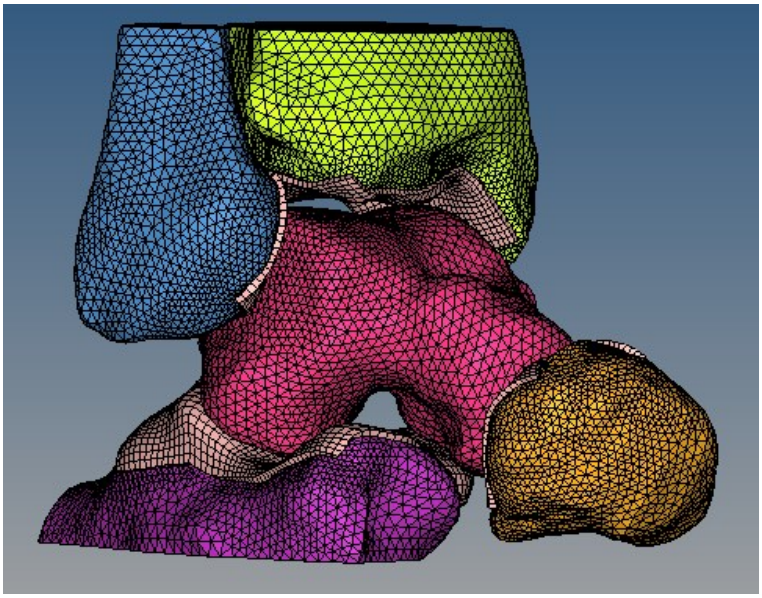

Figure 5-5: Mesh of the finite element model

The finite element model was exported into Abaqus (Abaqus 6.13, Dassault Systèmes Simulia Corp., Providence; RI, USA). The bone, biological and generic implant and cartilage structures were defined as the linear elastic material properties described in Table 5-1. Sets of three springs (k=20N/mm) located at the position of the anterior and posterior tibiofibular ligaments were added to the model to represent these ligaments. The cartilage and the corresponding bone elements were bonded together as they shared contact nodes at the surface.

Table 5-1: Assigned material properties in the FEA model

	E Young's Modulus (MPa)	**Poisson's ratio**
Bone	20,000 (Elias, et al. 2008) (Nigg and Herzog 1999)	0.3 (Parr, et al. 2013)
Implants - Titanium	119,000 (Elias, et al. 2008) (Karacali 2015)	0.32 (Karacali 2015)
Cartilage	12 (D. D. Anderson, J. K. Goldsworthy, et al. 2007)	0.42 (D. D. Anderson, J. K. Goldsworthy, et al. 2007)

The surrounding bones were brought into contact with the implants using a displacement-controlled method while the implant was fixed. The talus fixity was then released and the talus was allowed to move freely within the joint while the bones surrounding it remained fixed. At this point, the tibia and fibula were freed in the sagittal, transverse and coronal directions and loads of 200N were applied sequentially, using a force-controlled method, until a maximum of 2000N was reached. The model was validated by creating a secondary model based on the original that mimicked the boundary conditions and loading situation from Anderson et al (2007) to best compare results.

The DCM between the talar dome of the biological talus and implant was visually appraised and compared to the contact patterns/locations on the tibia and fibula cartilage when it came into contact (after 2000N was applied, as this was the largest load applied in the study and as such, generated the greatest contact areas and pressures) with biological talus versus the generic implant.

5.3 Results

5.3.1 Implant vs. Biological Talus: Geometric Comparison

The size distribution was as follows: four size 4, two size 5, two size 6, one size 7 and one size 9. When looking at the volumes of the right tali in the three positions, it was found that 6 of the 10 tali were on the cusp of two of the sizes found by Trovato et al (2016). The sizes and volumes of each subject are illustrated in Table 5-2.

Table 5-2: Sizes of implants

	Size		Volume (mm^2)	
Subject	**Left**	**Right**	**Left**	**Right**
1	7	7	43988	45679
4	4	4	30600	30034
5	4	4	31539	31412
9	6	5	38055	36596
11	6	6	37558	37504
16	5	6	36130	37685
17	9	9	54568	53367
18	4	4	29689	29309
22	4	4	30612	29072
24	5	6	36218	39331

The fibula- and tibia-talar dome articular surfaces between the implant and biological scans were modelled and the tibia and fibula were aligned. A typical DCM of the talar dome (when the tibia and fibula are aligned) is illustrated in Figure 5-6.

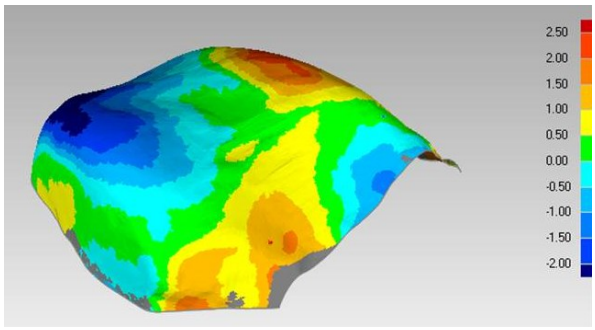

Figure 5-6: Deviation map of Subject 1 - biological talar dome vs implant talar dome in the neutral position

The positive and negative average-deviations (indicating that the implant surface is sitting outside/above or inside/below the biological talus surface respectively) on the talar dome are illustrated in Table 5-3 by subject and in Table 5-4 by position. The average among specimens (D_{avg}) positive and negative average-deviations for all subjects in all positions was 0.91mm and 0.70mm respectively.

Table 5-3: Average deviations of the implant from the biological talus on the talar dome for each subject

	Average Deviation (mm)	
Subject	**Positive**	**Negative**
1	0.94	0.99
4	1.06	0.45
5	0.83	0.77
9	1.19	1.24
11	0.87	0.72
16	0.97	0.64
17	0.74	0.62
18	0.89	0.66
22	0.88	0.40
24	0.74	0.52

Table 5-4: Average deviations (of the 10 subjects) of the implant from the biological talus on the talar dome for each position

	Average Deviation (mm)	
Position	**Positive**	**Negative**
Dorsi	0.99	0.72
Plantar	0.99	0.69
Neutral	0.75	0.70

The percentage of the talar dome within the acceptable range are illustrated in Table 5-5 by subject and in Table 5-6 by position.

Table 5-5: Deviations of implant from the biological talus on the talar dome for each subject

Subject	Percentage of Talar Dome between -0.5mm and 1.5mm deviation
1	61.76
4	77.39
5	64.28
9	53.97
11	72.35
16	71.33
17	76.81
18	69.65
22	81.37
24	81.04

Table 5-6: Deviations of the biological talus and implant on the talar dome for each position

Position	Percentage of Talar Dome between -0.5mm and 1.5mm deviation
Dorsi	67.96
Plantar	71.57
Neutral	73.45

5.4 Discussion

All 10 left ankles were scanned in the cadaver foot holder and modelled to obtain the sizes for the implants. The implants were 3D printed based on the models obtained from the CT scans of the left ankles. The left and right talus bones of humans have been found to be mirror images of one another (K. Islam, et al. 2014) and as such the contralateral talus can be used to determine the size and shape of the talus in need of replacement. The articulating surfaces on the talus are all important in considering a total talus bone replacement; however, the talar dome, which articulates with the tibia and fibula in the ankle joint, is of most importance because the ankle joint controls plantarflexion and dorsiflexion enabling the ability to walk (O'Rahilly 2008). Therefore, the focus of implant validation was on the talar dome. By assuming that the biological

talus is a perfect fit for the ankle, if the implant sits in the same position as the biological talus, the implant will be an acceptable fit. In order to investigate the position of the implant relative to the biological talus, the tibia and fibula from the biological talus scan were aligned with the tibia and fibula from the implant scan. Although small movement of the surrounding bone might occur while replacing the biological with implant talus we assumed that the location of the tibia and fibula remains unchanged and as such can be aligned. This enabled examining where the implant was positioned compared to the biological talus when the surrounding bones were aligned.

Typically the cartilage is about 1mm thick on the talar dome; however, considering that at this point we were not accounting for the opposite surface (in the plan for implantation); the decision was made to add 0.5mm globally around the talus. Additionally a 1mm shift is recognized as the determining criterion for relocation of the talus after injury (Lloyd, et al. 2006). Therefore, the implant could be considered to be in the same position as the biological talus if deviations were in the range of -0.5mm to 1.5mm. These percentages of the talar dome that lie within this acceptable range are illustrated by subject (Table 5-5) and position (Table 5-6). The results from average deviations indicate that the implant may be compatible. The positive D_{avg} of 0.91mm is well within the acceptable range (-0.5mm to 1.5mm). The 0.70mm negative D_{avg} is just outside the range indicating there may be issues with the implant sitting slightly too far inside from where the biological talus was. The implant sitting inside of the biological talus is less of a concern than the reverse as it will not interfere with the surrounding bones; however, it might alter the joint function due the gap between the talar dome and the fibula as the fibula has a role in ankle stability (Goh, et al. 1992). On average, 70% of the deviations on the talar dome between the biological talus and implant were within the acceptable range. This indicates that the geometric compatibility of the implant when in the ankle joint may be tolerable.

Dorsiflexion and plantarflexion take place between the talus and the tibia and fibula within the ankle mortise; therefore, this type of motion is of great importance to the study. The passive range of motion of the ankle is 20˚ dorsiflexion and 50˚ plantarflexion (Hoppenfeld 1976). The range of motion for the ankle joint that corresponds to normal walking is 10˚ dorsiflexion to 20˚ plantarflexion (Stauffer, Chao and RC 1977). Since the clinical objective of a talar body replacement is to restore the normal walking range of motion, it is important that our study

encompass that complete range. The dorsiflexion range was increased from 10˚ to 20˚ as 10˚ dorsiflexion is very near neutral and that small variation in range may not be as informative. As such, the range of 20˚ dorsiflexion to 20˚ plantarflexion was chosen as the range for this study. From Table 5-4 and Table 5-6 it is evident that the behaviour of the implant acts slightly different in the three different positions. The implant functions best in the neutral position and acts similarly in plantarflexion and dorsiflexion with less than a 3% difference between the two. This indicates that the implant may lead to a loss in joint compatibility as the ankle is put into more extreme ranges of motion.

Size discrepancies may be the cause of some of the poorer deviations as six of the tali were on the cusp of two different sizes (e.g. subject 9, size 5 for left foot and size 6 for right foot). These discrepancies may be because there is a small margin of error in the modelling process especially due to the fact that many of the scans showed osteopenic bones that are more difficult to model (likely due to the age of the cadavers). Results may be improved upon by either sizing up or down an implant accordingly. In a clinical setting, if a talus looks to be on the cusp, it may be practical to have two sizes on hand.

The DCMs obtained from the neutral position of subject 4 in this assessment were compared to contact pressure and location predicted in our FEA at an applied axial load of 2000N (Trovato et al, 2016). The 2000N was decided on as the impact forces on the talus during daily tasks are up to 2 to 3 times the body weight (Chi and Schmitt 2005) (Mahato and Murthy 2012). The contact areas of the tibia and fibula cartilage are shown alongside the DCM of the articular surface talar dome below in Figure 5-7 and Figure 5-8 respectively, for subject 4. The contact area on the tibia cartilage when in contact with the biological implant was more prevalent on the anterior lateral area and on the medial side of the surface (Figure 5-7). The contact area on the tibia cartilage when in contact with the generic implant was more prevalent on the posterior end and central anterior part of the surface (Figure 5-7). The contact area on the fibula cartilage when in contact with the biological implant was greater as there was no contact with the generic implant on the surface (Figure 5-8). The contact area, peak and mean contact pressures on the tibia and fibula articular cartilage when in contact with the biological and generic implants are shown in Table 5-7.

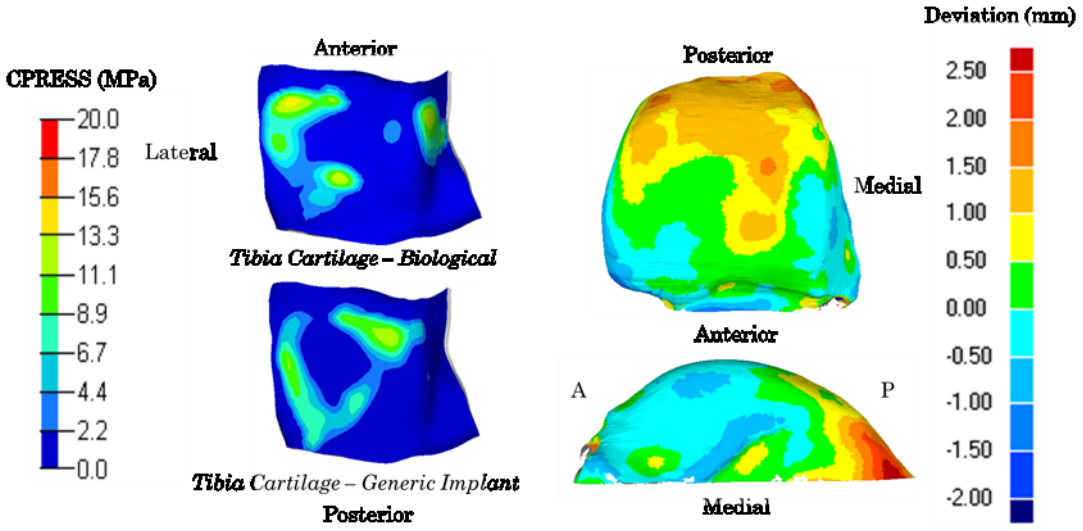

Figure 5-7: Subject 4 tibia cartilage contact (left) at 2000N and deviation map - biological talar dome vs. implant talar dome in the neutral position (right)

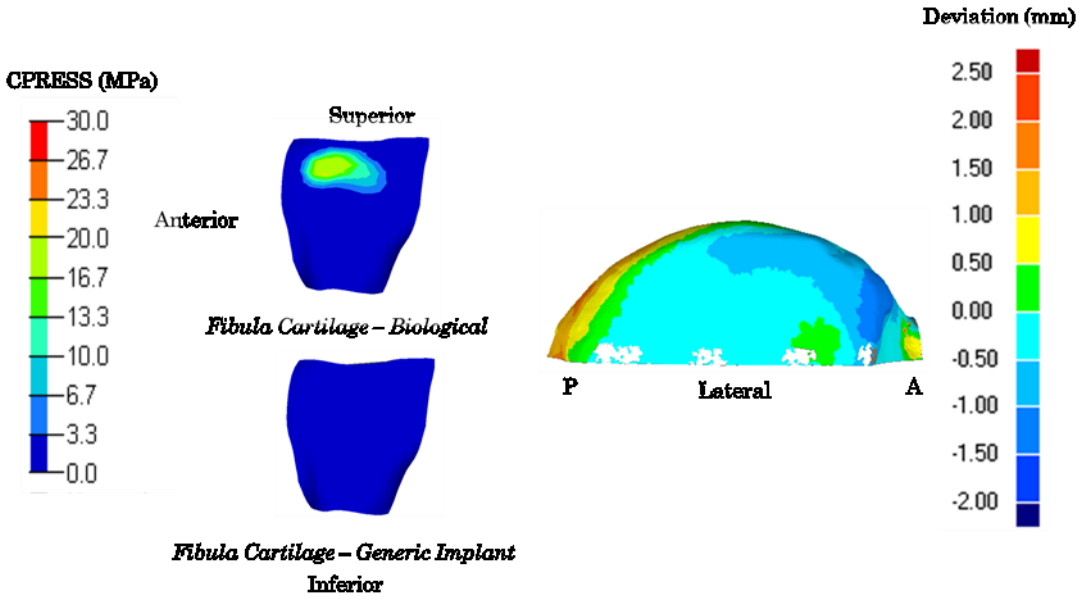

Figure 5-8: Subject 4 fibula cartilage contact (left) at 2000N and deviation map of lateral side- biological talar dome vs. implant talar dome in the neutral position (right)

Table 5-7: Subject 4 contact areas and pressures of the tibia and fibula articular cartilage when in contact with the biological and generic implants (modelled as titanium at 2000N of applied load)

Implant – Contact Location	Contact Area (mm^2)	Peak Contact Pressure (MPa)	Mean Contact Pressure (MPa)
Biological - Tibia	434.23	14.31	3.81
Generic - Tibia	446.73	12.97	3.30
Biological - Fibula	86.50	18.64	4.96
Generic - Fibula	0.00	0.00	0.00

The contact area on the tibia cartilage correlates to the biological talus sitting outside of the generic implant on both the lateral and medial sides of the anterior portion of the talar dome, and the generic implant sitting outside of the biological talus on the posterior end of the talar dome. The contact area on the fibula cartilage correlates to the biological talus sitting outside of the generic implant on the lateral side of the talar dome. This indicates that the geometric deviations (between the biological and generic implants) parallel the contact area predicted by of the FEA. As such, deviations can be used to predict where contact will occur.

No contact was detected on the fibula cartilage which indicates that the in-vivo location of the fibula may need to adjust when the implant is replaced with the biological talus as it has been shown that the tibiofibular joint may translate 1-3mm in a range of loading conditions (Scott, et al. 2007).

Although for some subjects deviations of the generic implant from the biological talus when sitting in the ankle mortise fell slightly out of the acceptable ranges, this cadaveric assessment appears promising. Results from comparing the deviation analysis to the FEA of subject 4 revealed we are able to use the deviation analysis to predict contact areas on the surrounding cartilage; and that the generic implant will not cause excessive contact pressures on the cartilage in the ankle joint.

From this study it appears that a generic implant chosen based on our earlier study revealed moderate functional and geometric compatibility of the ankle joint as compared to biological talus. A limitation of this study is that it only correlates the contact pattern to the deviation in the

one of the subjects in the neutral position, to further investigate this correlation it would be beneficial to analyze the joint in both plantar and dorsiflexion.

5.5 Conflict of Interest

There are no conflicts of interest to be reported for this publication.

5.6 Funding Source

Funding for this research was provided by Alberta Innovates Technology Futures and NSERC.

5.7 Acknowledgements

We would like to thank Shannon Stefaniuk, Carmen Thompson, and Heidi Corrigan at Medical Imaging Consultants, Century Park for assisting with the CT scanning process; and Hugh Barrett and Jason Papirny with the Anatomical Gifts Program at the University of Alberta for their assistance with the cadavers.

References

Anderson, Donald D., Jane K. Goldsworthy, Wendy Li, M. James Rudert, Yuki Tochigi, and Thomas D. Brown. 2007. "Physical validation of a patient-specific contact finite element model of the ankle." Journal of Biomechanics 1662-1669.

Barton, T, F Lintz, and I Winson. "Biomechanical changes associated with the osteoarthritic, arthrodesed, and prosthetic ankle joint." Foot Ankle Surg 17, no. 2 (June 2011): 52-7.

Bhandari, Mohit, and Anthony Adili. Evidence-based Orthopedics. Oxford: John Wiley & Sons, 2011.

Chi, Kai Jung, and Daniel Schmitt. "Mechanical energy and effective foot mass during impact loading of walking and running." Journal of Biomechanics 38 (2005): 1387-1395.

Elias, C.N, J.H.C. Lima, R. Valiev, and M.A. Meyers. "Biomedical Applications of Titanium and its Alloys." Journal of Materials, 2008: 46-49.

Goh, James, Joo Ang, Philippe Bayon, and Robert Pho. "Biomechanical Study on the Load-Bearing Characteristics of the Fibula and the Effects of Fiblar Resection." Clinical Orthopaedics and Related Research, no. 279 (1992): 223-8.

Haddad, SL, JC Coetzee, R Estok, K Fahrbach, D Banel, and L Nalysnyk. "Intermediate and long-term outcomes of total ankle arthroplasty and ankle arthrodesis. A systematic review of the literature." J Bone Joint Surg Am 89, no. 9 (September 2007): 1899-905.

Harnroongroj, T, and V Vanadurongwan. "The talar body prosthesis." J Bone Joint Surg Am. 79, no. 9 (Sep 1997): 1313-22.

Hoppenfeld, S. Physical Examination of the Spine and Extremities. East Norwalk, CT: Appleton-Century-Crofts, 1976.

Huang, PJ, and YM Cheng. "Delayed surgical treatment for neglected or mal-reduced talar fractures." Internal orthopaedics 29, no. 5 (Oct 2005): 326-9.

Islam, Kamrul, et al. "Three-dimensional geometric analysis of the talus for designing talar prosthetics." Journal of Engineering in Medicine 228, no. 4 (2014): 371-378.

Kakkar, Rahul, and MS Siddique. "Stresses in the ankle joint and total ankle replacement design." Foot and Ankle Surgery 17 (2011): 58-63.

Karacali, O. "Fatigue Analysis of Ti-55 Alloy Material for Multifunctional Surgical Instruments in Medical Engineering." 4th International Congress APMA. Fethiye, 2015. 1199-1201.

Lloyd, John, Sherief Elsayed, Kartik Hariharn, and Hiro Tanaka. "Revisiting the Concept of Talar Shift in Ankle Fractures." Foot Ankle Int 27, no. Oct (October 2006): 793-6.

Magnan, Bruno, Elisa Facci, and Pietro Bartolozzi. "Traumatic Loss of the Talus Treated with a Talar Body Prosthesis and Total Ankle Arthroplasty." The Journal of Bone and Joint Surgery, Incorporated 86-A, no. 8 (August 2004): 1778-82.

Mahato, Niladri Kumar, and Sathiya Narayana Murthy. "Articular and angular dimensions of the talus: inter-relationship and biomechanical significance." The Foot 22 (2012): 85-89.

Nigg, Benno, and Walter Herzog. Biomechanics of the Musculo-skeletal System. Baffins Lane, Chichester: John Wile & Sons Ltd, 1999.

O'Rahilly, Ronan. Basic Human Anatomy. Hanover, NH: Dartmouth Medical School, 2008.

Parr, W. C. H, U. Chamoli, A. Jones, W. R. Walsh, and S. Wroe. "Finite element micro-modelling of a human ankle bone reveals the importance of the trabecular network to mechanical performance: new methods for the generation and comparison of 3D models." Journal of Biomechanics 46 (2013): 200-205.

Santavirta, S, S Seitsalo, O Kiviluoto, and P Myllynen. "Fractures of the talus." J Trauma 24, no. 11 (Nov 1984): 986-9.

Scott, Jacob, Ho Lee, Wael Barsoum, and Antonie J van den Bogert. "The effect of tibiofemoral loading on proximal tibiofibular joint motion." Journal of Anatomy 211, no. 5 (2007): 647-53.

Stauffer, RN, EY Chao, and Brewster RC. "Force and motion analysis of the normal, diseased, and prosthetic ankle joint." Clin Orthop Relat Res 127 (1977): 189-96.

Stevens, Benjamin W., Christopher M. Dolan, John G. Anderson, and Charles D. Bukrey. "Custom Talar Prosthesis After Open Talar Extrusion in a Pediatric Patien." Foot & Ankle International, 2007: 933-8.

Tanaka, Y, et al. " Alumina ceramic talar body prosthesis for idiopathic aseptic necrosis of the talus." Key Engineering Materials, 2003: 805-8.

Thordarson, DB. "Talus fractures." FussSprungg 5 (2007): 104-13.

Trovato, A, M El-Rich, S Adeeb, and N Johma. "Finite Element Analysis of a Generic and Custom Talar Prosthetic with a Biological Talus." Journal of Biomechanics, 2016.

Trovato, A, M El-Rich, S Adeeb, and N Johma. 2016. "Geometric Analysis of the Talus and Development of a Generic Talar Prosthetic." *Foot and Ankle Surgery* Manuscript FAS-D-16-00068.

Chapter 6 - A Generic Talar Prosthesis for Bilateral Talar Collapse

Abstract

Background

Maintaining full ankle joint function after a talar injury remains a challenge using conventional treatments such as arthrodesis and total ankle arthroplasties. The majority of full talar implants are developed from the intact contralateral talus. If a patient does not have either talus intact, the use of a generic talar implant may be beneficial. This study explores the possibility of surgically implementing a generic talus bone prosthetic in a patient with bilateral talar avascular necrosis and collapse of the talar dome.

Methods

We have developed this generic implant in ten different sizes in a previous study. In addition to the generic implant, a custom implant was created using CT scans of the patient's talus, tibia and fibula. The biological talus and the implants (excluding the talar dome) were compared to determine how closely the intact part of the biological talus aligned with the implants. The talar domes of the implants were compared to the collapsed dome separately to determine how the width of the dome (implants), as well as the height of the dome (implants) differed from the collapsed (biological) talar dome. The extreme width of the biological talus and implants were also found to determine if the implants would fit in the ankle mortise.

Results

The implants were considered to be in the acceptable deviation range if the deviations on the articular surfaces were less than 1mm. The implant was found to be in the acceptable range.

Conclusions

Based on the analysis, we concluded that the custom implant or the generic size 4 implant would both be acceptable for implantation in the patient to maintain geometric compatibility of the ankle joint.

6.1 Background

Talar collapse due to avascular necrosis either spontaneous or post talar fracture, results in severe incongruity of the ankle joint resulting in pain, stiffness and disability. In the past, standard treatment for talar collapse has been surgical fusion of the tibia to the talus and the talus to the calcaneus (tibio-talo-calcaneal fusion). However, this course of treatment results in complete loss of motion and ankle and hindfoot function, and pseudarthrosis may develop resulting in further surgeries (Barton, Lintz and Winson 2011) (Dennison, et al. 2001) (Haddad, et al. 2007) (Hendrickx, et al. 2011). More recently, total ankle arthroplasties have been implemented with growing success; however, these arthroplasties are usually not an appropriate treatment for the collapse of the talar dome because the bone stock required for embedding the implant is insufficient (Hintermann and Valderrabano 2003).

A solution to the issues presented with arthrodesis and arthroplasties is a talar body implant that replaces the avascular portion of the talus or the talus in its entirety to maintain full ankle joint function. At this time, there have been reports of custom talar body replacements. All implants were custom made from various materials - stainless steel (Harnroongroj and Vanadurongwan 1997), alumina ceramic (Tanaka, et al. 2003), titanium alloy (Magnan, Facci and Bartolozzi 2004), and colbalt-chrome (B. W. Stevens, et al. 2007). The prosthesis developed by Harnroongroj and Vanadurongwan used custom measurements of volume and dimensions (including curvatures) of the contralateral talus. The prosthesis was a partial talar prosthesis consisting of the portion of the talus posterior to the talar neck, which was cemented to the existing talar head. It was successfully implanted in sixteen patients; however, some implants experienced loosening at the point of fixation. Tanaka et al. developed talar prostheses (for three patients) similar to that of Harnroongroj and Vanadurongwan (1997). They were based on anatomical features with reference to the contralateral normal talus. Magnan et al. (2004) produced a custom full talus and tibial plafond prosthesis using CT scans to determine the bone contours. The tibial component was fixed to the tibia and the talar implant was fixed to the calcaneus and navicular allowing ankle motion but eliminating subtalar and talonavicular motion. Both Stevens et al. (2007) and Taniguchi et al. (2015) created full talus prostheses that were not fixed to the surrounding bones. The implants were developed by utilizing CT scans to determine the geometry of the opposite talus bone. The prostheses were implanted in one, and

fifty-five ankles in the Stevens and Taniguchi studies respectively. All of the implants in the aforementioned studies were custom-made and as such, would typically involve increased time and expense. Additionally, all of the implants were based on measurements taken from the intact contralateral talus (with the exception of four cases in the Taniguchi study which based the implant on the less distorted talus). This required that at least one of the tali to be intact or predominantly intact; however, if both tali were deformed it would not be possible to create the implant based on the contralateral talus.

Two studies out of the University of Alberta developed a generic talus bone prosthetic in different sizes to mitigate the costs and the extended time between the onset of talar collapse and surgery (K. Islam, et al. 2014) (Trovato, El-Rich, et al. 2016). Ten unisex implant sizes for the talus bone were created to maintain geometric compatibility of the ankle joint. The implants were based on a sample size of 91 tali with 45% of the subjects being female, an implant shape that best fit all the tali, and used incremental jump in the cube root of the volume between sizes. The current study explores the possibility of surgically implementing this generic talus bone prosthetic in a patient wherein creating a custom implant may not be practical due to the fact that neither talus bones were intact. To achieve this, we assessed how the generic talus implants proposed by Trovato et al. (2016) compared to the biological collapsed talus as well as in comparison to a custom implant (that was developed based on the remaining intact part of the biological talus and the contour of the distal ends of the tibia and fibula).

6.2 Methods

A patient (female, age 53) presented with ankle pain (beginning in 2013) to the University of Alberta Hospital. The patient had a past history of oral corticosteroid use for Crohn's disease; however, the steroids were stopped in 2008. Radiographs and CT scans of both the left and right ankles were taken and revealed that she had developed bilateral talar avascular necrosis (AVN) and the dome on both her left and right tali had collapsed. She had a marked limp due to pain but maintained good ankle range of motion (approximately 75% of normal). There was generalized swelling and approximately 50% of normal subtalar motion. The right talus had worse collapse compared to the left and as such the right talus was chosen to be replaced first.

From the CT scan of the right ankle, DICOM images were imported into the 3D image processing software, MIMICS (Materialize NV, Belgium), and a 3D model was created. The model was then imported into Geomagic Control 2014 (Geomagic®, Morrisville, North Carolina; USA) for geometry cleaning, smoothing, and analysis.

The volume of the intact talus is required in order to select the proper implant size. The 3D model of the patient's talus was used to estimate the volume of the intact talus. The volume of the intact talus was calculated as the volume of the patient's biological talus as found in the CT scans from the patient's ankle plus volume added to account for the collapse of the talar dome. The volume of the collapsed area was calculated by determining the surface area (540mm^2) of the collapsed area (Figure 6-1) and multiplying it by the estimated depth of the collapse (1mm). Because the volume of the intact talus was an estimate, the talus was then compared to the implant sizes within a close range of the predicted size.

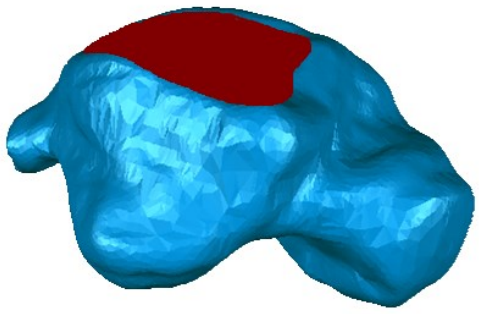

Figure 6-1: Area of collapsed talar dome

The CT scans of the patient's talus, tibia, and fibula were also used to create a custom implant of the talus. The custom implant was created by keeping the intact portion of the biological talus and creating an approximated talar dome by extracting the three-dimensional CAD file of the patient talus bone from medical CT data using MIMICS software (Materilaise, Leuven, Belgium). This resultant digital data was imported in to Freeform Modeling Plus software (3D Sytems, Rock Hill, South Carolins, USA). A suitable donor talus was also imported and then rescaled to match the dimensions of the patient talus. The donor shape was then aligned over the patient talus and the dome portion of the rescaled donor talus was merged with the intact portion

of the patient talus. The shape was further adjusted to give a more custom fit to articulate with the patient's tibial plafond and fibula articulating surfaces.

Prior to any analysis of the biological talus and the implants, the calculated biological talus size was increased by 0.5mm all around to account for cartilage thickness. This was because all of the implants had accounted for cartilage in their design and the biologic talus size was determined using a CT scan which does not image the cartilage. The biological talus and implants were then segmented into two sections – the talar dome and remaining intact talus. This was achieved by creating three planes at the extreme anterior, posterior and distal ends of the tibia as shown on the CT scans. These formed cutting planes and were used to isolate the talar dome from the intact part of the talus (Figure 6-2, Figure 6-3). The generic and custom implants were aligned to the intact portion of the biological talus (the talus excluding the talar dome) using the best-fit approach built into Geomagic. Once aligned, the talus and the implants (excluding the talar dome) were compared to determine how closely the intact part of the biological talus aligned with the implants. The talar domes of the implant were then compared to the collapsed dome separately to determine how the width of the dome as well as the height of the dome differed from the collapsed talar dome. The extreme width of the biological talus and the two implants (generic and custom) were found and compared as well to ensure that the implant would not be too large to fit between the tibia and fibula. This was done by fitting a bounding box (a wire-framed box that indicates the maximum extents of an object) surrounding the talus with the box edges at the distal, proximal, medial, lateral, anterior and posterior edges of the talus as shown on the CT scans. The comparisons were carried out using the Geomagic 3D Compare Analysis and deviation contour maps (DCMs) were created.

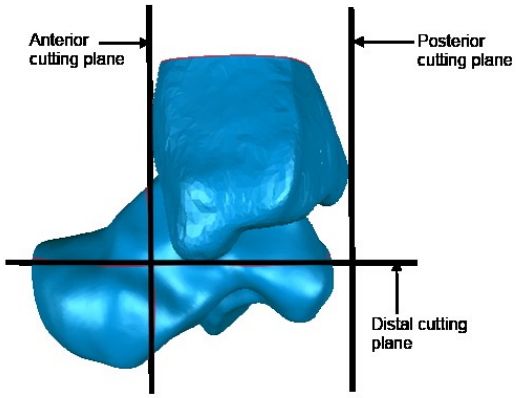

Figure 6-2: Cutting planes

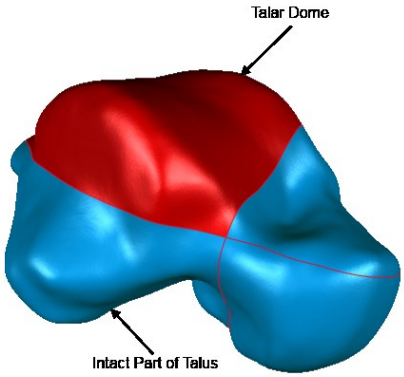

Figure 6-3: Segmented talus

6.3 Results

The volume of the collapsed biological talus was found to be 33,248mm^3. When including the approximation of the area lost from the dome collapse, the predicted volume of the intact biological talus was 33,788mm^3. The volume range for size 4 was 28,906mm^3 to 32,964mm^3 and the volume range for size 5 was 32,964mm^3 to 37,384mm^3. From the predicted volume of the intact talus, a size 5 was selected for analysis; however, because of the close proximity of the predicted volume to the cusp of the size cut-off between sizes 4 and 5, size 4 was also selected for analysis. DCMs comparing the intact portion of the biological talus with sizes 4, 5 and the

custom implant are illustrated in Figure 6-4, Figure 6-5, and Figure 6-6 respectively. The average deviations between the intact portion of the biological talus and sizes 4, 5 and the custom implant are shown in Table 6-1.

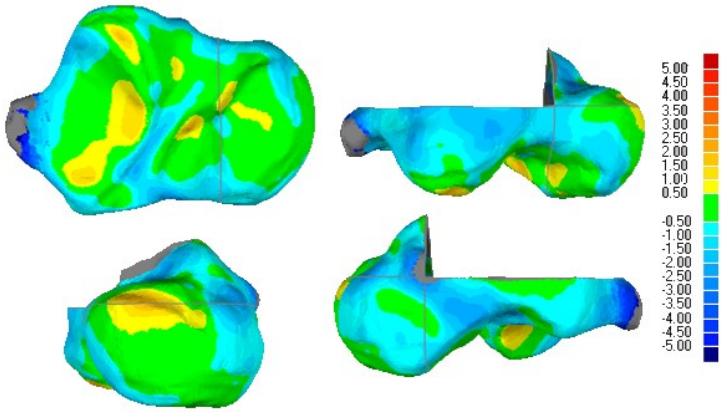

Figure 6-4: Deviation map of intact biological talus vs size 4 (views clockwise starting from top left: distal, lateral, medial, anterior)

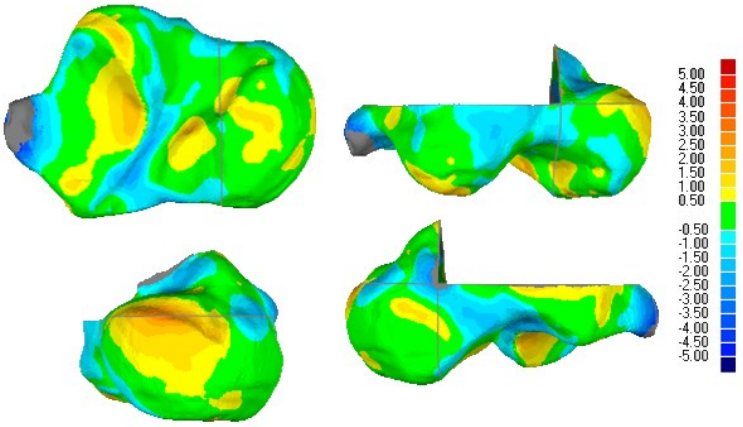

Figure 6-5: Deviation map of intact biological talus vs size 5 (views clockwise starting from top left: distal, lateral, medial, anterior)

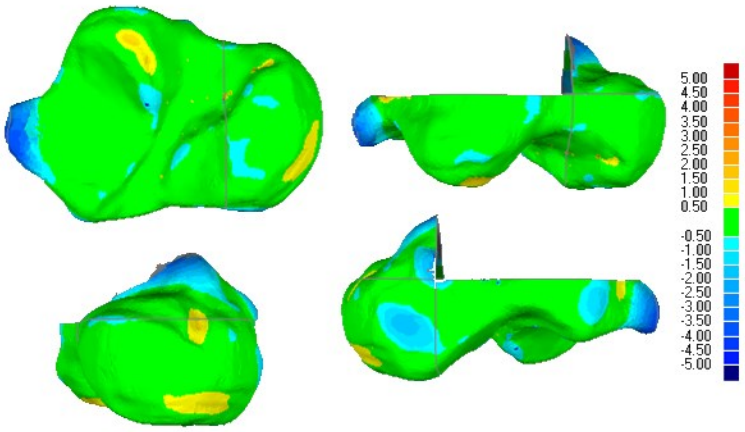

Figure 6-6: Deviation map of intact biological talus vs custom implant (views clockwise starting from top left: distal, lateral, medial, anterior)

Table 6-1: Average deviations between the intact portion of the biological talus vs the implants

Implant (Intact)	Average Positive Deviation (mm)	Average Negative Deviation (mm)
Size 4	0.51	-0.88
Size 5	0.64	-0.70
Custom	0.24	-0.37

DCMs comparing the talar dome of the biological talus with sizes 4, 5 and the custom implant are illustrated in Figure 6-7, Figure 6-8, and Figure 6-9 respectively. The average positive deviations between the biological talar dome and the talar dome of sizes 4, 5 and the custom implant are shown in Table 6-2. The extreme widths of the biological talus, size 4, size 5 and custom implant were 39.6mm, 39.3mm, 41.1mm and 38.7mm respectively.

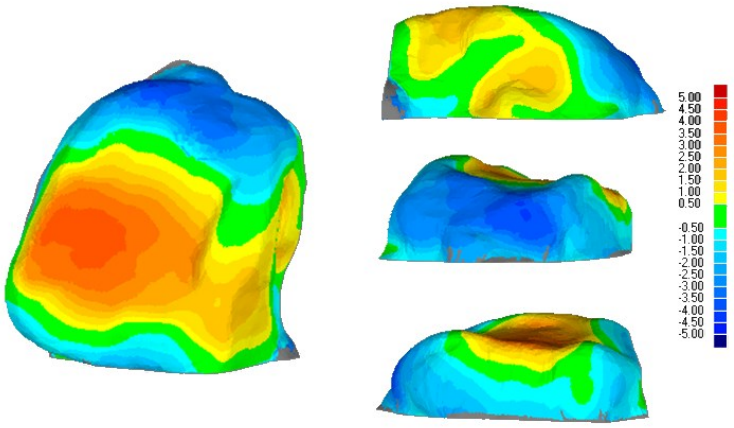

Figure 6-7: Deviation map of the talar dome of the biological talus vs size 4 (views clockwise starting from top left: proximal, medial, posterior, lateral)

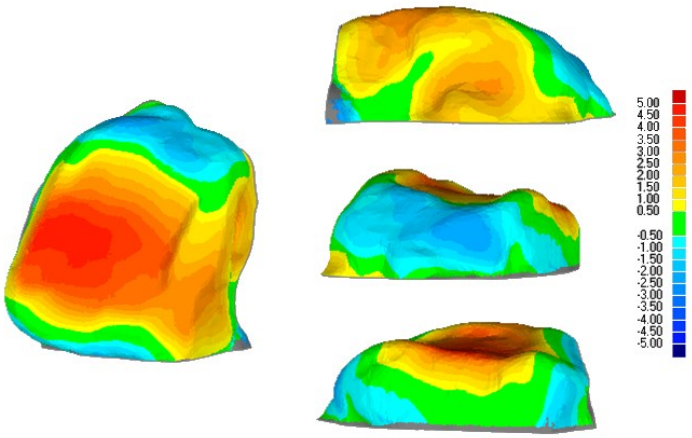

Figure 6-8: Deviation map of the talar dome of the biological talus vs size 5 (views clockwise starting from top left: proximal, medial, posterior, lateral)

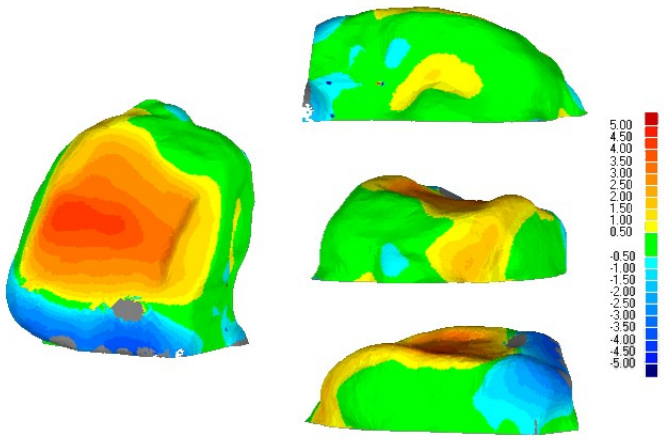

Figure 6-9: Deviation map of the talar dome of the biological talus vs custom implant (views clockwise starting from top left: proximal, medial, posterior, lateral)

Table 6-2: Average deviations between the talar dome of the biological talus vs the implants

Implant (Dome Only)	Average Positive Deviation (mm)
Size 4	1.45
Size 5	1.91
Custom	1.38

6.4 Discussion

Throughout the past decades, there has been significant progression in treating talar injuries. The field of study has advanced from mobility limiting arthrodesis to total ankle arthroplasties and more currently, custom made prosthetics. Custom prosthetics have enabled patients to experience fuller ranges of motion than in the past but are not without their drawbacks. Custom implants take more time to develop and can often be expensive. Additionally, custom implants are often modelled from the contralateral talus; this becomes an issue if the contralateral talus is not intact (Harnroongroj and Vanadurongwan 1997) (Tanaka, et al. 2003) (Taniguchi, Takakura and Tanaka, et al. 2015). To our knowledge, this is the first study to propose using a generic implant in a patient presenting with bilateral AVN and collapse of the talar dome.

The only portion of the patient's talus that was deformed was the talar dome; as such, the rest of the talus (the intact portion of the talus) was assumed to be functionally articulating with the

calcaneus and the navicular. Implants were considered to be in the acceptable deviation range if the deviations on the articular surfaces were less than 1mm as a 1mm shift was recognized as the determining criterion for reduction of the talus after injury (Lloyd, et al. 2006). As such, the deviations on the articular surfaces of the implants when compared to the intact biological talus should be within the specified ±1.0mm criteria to function similarly. The average deviations between the implants and the intact portion of the biological talus were all within this range as shown in Table 6-1. The custom implant had the least deviations between itself and the biological talus with 95% being within ±1.0mm deviation criteria and the majority of the deviations on the calcaneal and navicular articulating surface being within the acceptable range (Figure 6-6). This is to be expected because the intact portion of the custom implant was modelled from the biological talus and as such, they should be identical. Of the two generic sizes, size 4 was found to be a better fit than size 5 on the intact portion of the talus. Although size 4 had higher deviations on the overall intact portion of the talus with 70% of the deviations being within the acceptable criteria as compared to 78% with size 5; based on the deviations observed in Figure 6-4 and Figure 6-5 size 4 was deemed to be a better fit. This is because on the calcaneal and navicular surfaces, the majority of the deviations between size 4 and the biological talus were within the acceptable range on these surfaces whereas size 5 had more deviations outside this range, especially on the navicular articulating surface. The analysis of the articulating surfaces on the intact portion of the talus indicated that although the custom implant had lower deviations, the generic size 4 was still within the acceptable range and would be able to articulate well with the calcaneus and navicular.

Analysis of the talar dome showed that the custom implant was undersized at the anterior portion of the talar dome (indicated by the blue on Figure 6-9) and the generic implants were undersized at the posterior portion of the talar dome (indicated by the blue on Figure 6-7 and Figure 6-8). Table 6-2 indicates that size 4 and the custom implant have the most similar talar domes with the average positive deviations being 1.45mm and 1.38mm respectively compared to 1.91mm for size 5. This indicates that size 5 would have a higher talar dome than the custom implant or size 4. This is visually confirmed by observing the top of the talar dome in Figure 6-7, Figure 6-8, and Figure 6-9. The extreme width of the biological talar dome was found to be 39.6mm. Both the custom implant and size 4 were under this threshold with size 4 having the closest width. Size 5 was above this threshold by 1.5mm indicating that it would be too wide for the ankle

mortise. This is again visually confirmed by the medial yellow region of the talar dome shown in Figure 6-8. This indicates that size 5 is outside the biological dome (and it is not offset by any deviations on the lateral side). The analysis of the talar dome indicated that size 5 will likely be too tall and wide for the ankle mortise and that custom implant or size 4 would both be acceptable.

6.5 Conclusion

Based on this analysis, we concluded that the custom implant or size 4 would both be acceptable for implantation in the test subject to maintain geometric compatibility of the ankle joint. Size 4 would be preferred as generic implants are faster and more cost effective to develop. Additionally, because the patient presented with bilateral talar AVN, the custom implant is a best guess to the shape of the talar dome and not based on actual geometry of the talus. Future studies include finite element analysis to determine whether or not a generic implant is sufficient to maintain both functional and geometric compatibility of the ankle joint.

6.6 Ethics Statement

Ethics approval has been obtained from the Health Research Ethics Board.

6.7 Conflict of Interest

There are no conflicts of interest to be reported for this publication.

6.8 Funding Source

Funding for this research is provided by Alberta Innovates Technology Futures and NSERC.

References

Barton, T, F Lintz, and I Winson. "Biomechanical changes associated with the osteoarthritic, arthrodesed, and prosthetic ankle joint." Foot Ankle Surg 17, no. 2 (June 2011): 52-7.

Dennison MG, Pool RD, Simonis RB, Singh BS. "Tibiocalcaneal fusion for avascular necrosis of the talus." Bone Joint Surg Br, no. 83(2) (2001): 199-203.

Haddad, SL, JC Coetzee, R Estok, K Fahrbach, D Banel, and L Nalysnyk. "Intermediate and long-term outcomes of total ankle arthroplasty and ankle arthrodesis. A systematic review of the literature." J Bone Joint Surg Am 89, no. 9 (September 2007): 1899-905.

Harnroongroj, T, and V Vanadurongwan. "The talar body prosthesis." J Bone Joint Surg Am. 79, no. 9 (Sep 1997): 1313-22.

Hendrickx, RP, SA Stufkens, EE de Bruijn, IN Sierevelt, C van Dijk, and GM Kerkhoffs. "Medium- to long-term outcome of ankle arthrodesis." Foot Ankle Int 32, no. 10 (October 2011): 940-7.

Hintermann, Beat, MD, and Victor, MD Valderrabano. "Total Ankle Replacement." Foot Ankle Clin 8, no. 2 (June 2003): 375-405.

Islam, K, et al. "Three-dimensional geometric analysis of the talus for designing talar prosthetics." Proceedings of the 2014 combined Canadian Orthopaedic Association/American Orthopaedic Association (COA/AOA) and the Canadian Orthopaedic Research Society (CORS) Annual Meeting. Montreal: The Canadian Orthopaedic Association, 2014. 371-8.

Lloyd, John, Sherief Elsayed, Kartik Hariharn, and Hiro Tanaka. "Revisiting the Concept of Talar Shift in Ankle Fractures." Foot Ankle Int 27, no. Oct (October 2006): 793-6.

Magnan, Bruno, Elisa Facci, and Pietro Bartolozzi. "Traumatic Loss of the Talus Treated with a Talar Body Prosthesis and Total Ankle Arthroplasty." The Journal of Bone and Joint Surgery, Incorporated 86-A, no. 8 (August 2004): 1778-82.

Stevens, Benjamin W., Christopher M. Dolan, John G. Anderson, and Charles D. Bukrey. "Custom Talar Prosthesis After Open Talar Extrusion in a Pediatric Patien." Foot & Ankle International, 2007: 933-8.

Tanaka, Y, et al. " Alumina ceramic talar body prosthesis for idiopathic aseptic necrosis of the talus." Key Engineering Materials, 2003: 805-8.

Taniguchi, A., et al. "An Alumina Ceramic Total Talar Prosthesis for Osteonecrosis of the Talus." J Bone Joint Surg Am, no. 97 (2015): 1348-53.

Trovato, A, M El-Rich, S Adeeb, and N Johma. 2016. "Geometric Analysis of the Talus and Development of a Generic Talar Prosthetic." *Foot and Ankle Surgery* Manuscript FAS-D-16-00068.

Chapter 7 – Summary and Conclusions

7.1 Summary and Conclusions

This research aimed at understanding how a generic talar implant would function for patients in need of a talar replacement.

Comparisons of 91 male and female tali were conducted to determine if tali had different shapes among the human population and between sexes. No shape differences were found. As a result, a generic unisex implant in ten sizes was created and validated by geometrically comparing the generic implants with the population in this study.

A 3D nonlinear FE model of the talus and surrounding bones was created and validated against experimental studies. The model determined the contact pressures and contact areas on the cartilage surfaces surrounding the talus caused by loading the tibia and fibula to 2000N of load when a biological talus, custom implant, or generic implant were in the ankle mortise. The results indicated that the contact pressures caused by the custom implant were much higher than that caused by the biological talus and the generic implant caused contact pressures more similar to the biological talus. The contact patterns caused by the custom implant were similar but smaller than the contact patterns from the biological talus. The contact patterns were similar in magnitude but slightly different in location from that of the biological talus when the generic implant was placed in the joint.

A cadaveric assessment was carried out to determine geometric joint compatibility of the generic implant versus the biological talus; and to see if the deviations from the geometric assessment were associated with the contact pressure patterns from the FEA. Seventy percent of the deviations on the talar dome between the biological talus and generic implant were within the acceptable range. The deviations patterns were linked to the contact patterns caused by a 2000N axial load applied to the tibia and fibula.

A case study was conducted on a patient with bilateral talar avascular necrosis and collapse of the talar dome to determine if a generic implant would function the same as a custom implant. The generic and custom implants were found to be in the acceptable deviation range of 1mm, and it was determined that either would be acceptable for implantation in the patient to maintain geometric compatibility of the ankle joint.

This research demonstrates through FEA and geometric analysis that a generic talar implant may be a viable option for those in need of a talar replacement.

7.2 Recommendations for Future Research

The following are recommendations for future research in this area:

- Cartilage thickness on the tibia, fibula, calcaneus and navicular could be investigated more thoroughly by incorporating patient specific MRI data into FE models.
- Including more specimens in the FE models would be beneficial to compare with this model.
- Comparison of the contact pressures and areas in dorsiflexion and plantarflexion would be beneficial to see if the patterns and pressures vary in different positions.

Bibliography

Adeeb, Samer, Ezzeldin Y. Sayed Ahmed, John Matyas, David A. Hart, and Cyril B. Frank. 2004. "Congruency effects on load bearing in diarthrodial joints." *Computer Methods in Biomechanics and Biomedical Engineering* 7 (3): 147-157.

Anderson, Donald D., Jane K. Goldsworthy, Kiran Shivanna, Nicole M. Grosland, Douglas R. Pedersen, Thaddeus P. Thomas, Yuki Tochigi, J. Lawrence Marsh, and Thomas D. Brown. 2006. "Intra-articular contact stress distributions at the ankle throughout stance phase--patient-specific finite element analysis as a metric of degeneration propensity." *Biomech Model Mechanobiol.* 5 (2-3): 82-89.

Anderson, Donald D., Jane K. Goldsworthy, Wendy Li, M. James Rudert, Yuki Tochigi, and Thomas D. Brown. 2007. "Physical validation of a patient-specific contact finite element model of the ankle." *Journal of Biomechanics* 1662-1669.

Barton, T, F Lintz, and I Winson. 2011. "Biomechanical changes associated with the osteoarthritic, arthrodesed, and prosthetic ankle joint." *Foot Ankle Surg* 17 (2): 52-7.

Bhandari, Mohit, and Anthony Adili. 2011. *Evidence-based Orthopedics.* Oxford: John Wiley & Sons.

Carr, James B. 2009. "Malleolar Fractures and Soft Tissue Injuries of the Ankle." In *Skeletal Trauma, Fourth Edition*, by Bruce D. Browner, Jesse B. Jupiter, Alan M. Levine, Peter G. Trafton and Christian Krettek, 2515-2584. Philadelphia, PA: SAUNDERS ELSEVIER.

Cheung, Jason Tak Man, Ming Zhang, Aaron Kam-Lun Leung, and Yu-Bo Fan. 2005. "Three-dimensional finite element analysis of the foot during standing--a material sensitivity study." *Journal of Biomechanics* 38: 1045-1054.

Chi, Kai Jung, and Daniel Schmitt. 2005. "Mechanical energy and effective foot mass during impact loading of walking and running." *Journal of Biomechanics* 38: 1387-1395.

Davis, R.H., C.J. Twining, T.F. Cootes, J.C. Waterton, and C.J. Taylor. 2002. "3D Statistical Shape Models Using Direct Length." *Computer Vision — ECCV*, April 29: 3-20.

Dennison, MG, RD Pool, RB Simonis, and BS Singh. 2001. "Tibiocalcaneal fusion for avascular necrosis of the talus." *Bone Joint Surg Br* (83(2)): 199-203.

Early, John S. 2008. "Talus Fracture Management." *Foot Ankle Clin N Am* 13: 635-657.

Elias, C.N, J.H.C. Lima, R. Valiev, and M.A. Meyers. 2008. "Biomedical Applications of Titanium and its Alloys." *Journal of Materials* 46-49.

Ferrari, J, DA Hopkinson, and AD Linney. 2004. "Size and shape differences between male and female foot bones: is the female foot predisposed to hallux abducto valgus deformity." *Journal of the American Podiatric Medical Association* 94 (5): 434-52.

Fregly, B.J., S.A. Banks, D.D. D'Lima, and C.W. Colwell. 2008. "Sensitivity of knee replacement contact calculations to kinematic measurement errors." *J. Orthop. Res.* 1173–1179.

Goh, James, Joo Ang, Philippe Bayon, and Robert Pho. 1992. "Biomechanical Study on the Load-Bearing Characteristics of the Fibula and the Effects of Fiblar Resection." *Clinical Orthopaedics and Related Research* (279): 223-8.

Haddad, SL, JC Coetzee, R Estok, K Fahrbach, D Banel, and L Nalysnyk. 2007. "Intermediate and long-term outcomes of total ankle arthroplasty and ankle arthrodesis. A systematic review of the literature." *J Bone Joint Surg Am* 89 (9): 1899-905.

Harnroongroj, T, and V Vanadurongwan. 1997. "The talar body prosthesis." *J Bone Joint Surg Am.* 79 (9): 1313-22.

Hayes, A, Y Tochigi, and CL Saltzman. 2006. "Ankle morphometry on 3D-CT images." *The Iowa orthopaedic journal* 26: 1-4.

Hendrickx, RP, SA Stufkens, EE de Bruijn, IN Sierevelt, C van Dijk, and GM Kerkhoffs. 2011. "Medium- to long-term outcome of ankle arthrodesis." *Foot Ankle Int* 32 (10): 940-7.

Hintermann, Beat, MD, and Victor, MD Valderrabano. 2003. "Total Ankle Replacement." *Foot Ankle Clin* 8 (2): 375-405.

Hoppenfeld, S. 1976. *Physical Examination of the Spine and Extremities.* East Norwalk, CT: Appleton-Century-Crofts.

Huang, PJ, and YM Cheng. 2005. "Delayed surgical treatment for neglected or mal-reduced talar fractures." *Internal orthopaedics* 29 (5): 326-9.

Islam, K, A Dobbe, K Duke, M El-Rich, S Dhillon, S Adeeb, and NM Jomha. 2014. "Three-dimensional geometric analysis of the talus for designing talar prosthetics." *Proceedings of the 2014 combined Canadian Orthopaedic Association/American Orthopaedic Association (COA/AOA) and the Canadian Orthopaedic Research Society (CORS) Annual Meeting.* Montreal: The Canadian Orthopaedic Association. 371-8.

Islam, K., A. Dobbe, A. Komeili, K. Duke, M. El-Rich, S. Dhillon, S. Adeeb, and N. M. Jomha. 2014. "Symmetry analysis of talus bone: A Geometric morphometric approach." *Bone and Joint Research* 3 (5): 139-145.

Islam, Kamrul, Ashlee Dobbe, Kajsa Duke, Marwan El-Rich, Sukhvinder Dhillon, Samer Adeeb, and Nadr M. Jomha. 2014. "Three-dimensional geometric analysis of the talus for designing talar prosthetics." *Journal of Engineering in Medicine* 228 (4): 371-378.

Kakkar, Rahul, and MS Siddique. 2011. "Stresses in the ankle joint and total ankle replacement design." *Foot and Ankle Surgery* 17: 58-63.

Kapandji, AI. 2011. *The Physiology of the Joints Volume Two The Lower Limb.* Toronto: Elsevier.

Karacali, O. 2015. "Fatigue Analysis of Ti-55 Alloy Material for Multifunctional Surgical Instruments in Medical Engineering." *4th International Congress APMA.* Fethiye. 1199-1201.

Kimizuka, Mamori, and Hisashi, Fukubayyashi, Toru Kurosawa. 1980. "Load-bearing Pattern of the Ankle Joint." *Archives of Orthopaedic and Trauma Surgery* 45-49.

Konrath, Gregory A., Andrew J. Hamel, Steve A. Olson, Brian Bay, and Neil A. Sharkey. 1998. "The role of the acetabular labrum and the transverse acetabular ligament in load transmission in the hip." *The Journal of Bone and Joint Surgery* 80-A (12): 1781-1788.

Lloyd, John, Sherief Elsayed, Kartik Hariharn, and Hiro Tanaka. 2006. "Revisiting the Concept of Talar Shift in Ankle Fractures." *Foot Ankle Int* 27 (Oct): 793-6.

Magnan, Bruno, Elisa Facci, and Pietro Bartolozzi. 2004. "Traumatic Loss of the Talus Treated with a Talar Body Prosthesis and Total Ankle Arthroplasty." *The Journal of Bone and Joint Surgery, Incorporated* 86-A (8): 1778-82.

Mahato, N. 2011. "Morphology of sustentaculum tali: Biomechanical importance and correlation with angluar dimensions of the talus." *The Foot* 21: 179-83.

Mahato, Niladri Kumar, and Sathiya Narayana Murthy. 2012. "Articular and angular dimensions of the talus: inter-relationship and biomechanical significance." *The Foot* 22: 85-89.

Martini, Frederic H., Michael J. Timmons, and Robert B. Tallitsch. 2006. *Human Anatomy.* Fifth. San Francisco: Pearson Education Inc.

Millington, S.A., M. Grabner, R. Wozelka, D.D. Anderson, S.R. Hurwitz, and J.R. Crandall. 2007. "Quantification of ankle articular cartilage topography and thickness using a high resolution stereophotography system." *OsteoArthritis and Cartilage* 205-211.

Nigg, Benno, and Walter Herzog. 1999. *Biomechanics of the Musculo-skeletal System.* Baffins Lane, Chichester: John Wile & Sons Ltd.

O'Rahilly, Ronan. 2008. *Basic Human Anatomy.* Hanover, NH: Dartmouth Medical School.

Ozen, Mustafa, Onur Sayman, and Hasan Havitcioglu. 2013. "Modeling and stress analyses of a normal foot-ankle and a prosthetic foot-ankle complex." *ACTA of Bioengineering and Biomechanics* 15 (3): 19-27.

Ozkan, Arif, Halil Atmaca, Ibrahim Mutlu, Talip Celik, Levent Ugur, and Yasin Kisioglu. 2013. "Stress distribution comparisons of foot bones in patient with tibia vara: a finite element study." *Acta of Bioengineering and Biomechanics* 15 (4): 67-72.

Parr, W. C. H, U. Chamoli, A. Jones, W. R. Walsh, and S. Wroe. 2013. "Finite element micro-modelling of a human ankle bone reveals the importance of the trabecular network to

mechanical performance: new methods for the generation and comparison of 3D models." *Journal of Biomechanics* 46: 200-205.

Pena, E., B. Calvo, M.A. Martinez, and M. Doblare. 2005. "A three-dimensional finite element analysis of the combined behavior of ligaments and menisci in the healthy human knee joint." *Journal of Biomechanics* 39: 1686-1701.

Santavirta, S, S Seitsalo, O Kiviluoto, and P Myllynen. 1984. "Fractures of the talus." *J Trauma* 24 (11): 986-9.

Scott, Jacob, Ho Lee, Wael Barsoum, and Antonie J van den Bogert. 2007. "The effect of tibiofemoral loading on proximal tibiofibular joint motion." *Journal of Anatomy* 211 (5): 647-53.

Smith, Patrick N., and Bruce H. Ziran. 1999. "Fractures of the Talus." *Operative Techniques in Orthopaedics* 9 (3): 229-38.

Stagni, R, A Leardini, A Ensini, and A Cappello. 2005. "Ankle morphometry evaluated using a new semi automated technique based on X-ray pictures." *Clinical biomechanics* 20 (3): 307-11.

Stagni, R, A Leardini, F Catani, and A Cappello. 2004. "A new semi-automated measurement technique based on X-ray pictures for ankle morphometry." *J Biomech* 37 (7): 1113-8.

Stauffer, RN, EY Chao, and Brewster RC. 1977. "Force and motion analysis of the normal, diseased, and prosthetic ankle joint." *Clin Orthop Relat Res* 127: 189-96.

Stevens, B. W., C. M. Dolan, J. G. Anderson, and C. D. Bukrey. 2007. "Custom talar prosthesis after open talar extrusion in a pediatric patient." *Foot Ankle International* 28 (8): 933-938.

Tanaka, Y, Y Takakura, K Kadono, A Taniguchi, K Hayashi, J Iida, K Sugimoto, Y Tohma, and H Ohgushi. 2003. " Alumina ceramic talar body prosthesis for idiopathic aseptic necrosis of the talus." *Key Engineering Materials* 805-8.

Taniguchi, A., Y. Takakura, K. Sugimoto, K. Hayashi, K. Ouchi, T. Kumai, and Y. Tanaka. 2012. "The use of a ceramic talar body prosthesis in patients with aseptic necrosis of the talus." *The Journal of Bone and Joint Surgery* 94-B (11): 1529-1533.

Taniguchi, A., Y. Takakura, Y. Tanaka, H. Kurokawa, K. Tomiwa, T. Matsuda, T. Kumai, and K. Sugimoto. 2015. "An Alumina Ceramic Total Talar Prosthesis for Osteonecrosis of the Talus." *J Bone Joint Surg Am* (97): 1348-53.

Thordarson, DB. 2007. "Talus fractures." *FussSprungg* 5: 104-13.

Trovato, A, M El-Rich, S Adeeb, and N Johma. 2016. "Finite Element Analysis of a Generic and Custom Talar Prosthetic with a Biological Talus." *Journal of Biomechanics.*

Trovato, A, M El-Rich, S Adeeb, and N Johma. 2016. "Geometric Analysis of the Talus and Development of a Generic Talar Prosthetic." *Foot and Ankle Surgery* Manuscript FAS-D-16-00068.

Zhang, K.Y., A Wiktorowicz-Conroy, J.R. Hutchinson, M Doube, M Klosowski, S.J. Shefelbine, and A.M. Bull. 2012. "3D Morphometric and Posture Study of Felid Scapulae Using Statistical Shape ModellingX." *PLoS One* 7 (4).